Search for $t\bar{t}HH$ in the semileptonic decay of the top pair and the Higgs pair decay into b-quarks, using the 2017 data sample

Leônidas Fernandes do Prado,[1,2] Karim El Morabit,[3] Philip Keicher,[3] Aurore Savoy-Navarro,[1] Matthias Schröder,[3] Jan van der Linden,[3] and Michael Waßmer[3]

[1]IRFU - CEA, University Paris-Saclay, DPhP and CNRS/IN2P3, France

[2]Instituto de Física Teórica – UNESP, São Paulo, Brazil

[3]Karlsruhe Institute of Technology, Germany

E-mail: leonidas.prado@cern.ch, karim.el.morabit@cern.ch, philip.keicher@kit.edu, aurore.savoy.navarro@cern.ch, matthias.schroeder@kit.edu, jan.linden@student.kit.edu, michael.wassmer@cern.ch

Abstract. This note documents the results of the search for the production of a top quark-antiquark pair associated to a pair of Higgs bosons, using the full proton-proton collision data set corresponding to an integrated luminosity of approximately 41.5 fb^{-1} recorded with the CMS experiment at a center-of-mass energy of 13 TeV collected in 2017. This is the first time this search is performed with real data. The cross-section as predicted by the Standard Model is of 0.775 fb. The candidate $t\bar{t}HH$ events are selected with criteria enhancing the lepton+jets decay channels of the $t\bar{t}$ system and the decay of the double Higgs bosons into two bottom quark-antiquark pairs. Starting from the $t\bar{t}H$ analysis framework with the 2017 data, new developments are introduced to perform the search for this new signal. In order to increase the sensitivity of the search, selected events are split into several categories with different expected signal and background rates. A combined fit of multivariate discriminant templates across all categories to data is performed to extract the result. The best-fit μ value achieved with Asimov data, this specific signature and 2017 luminosity is: $1^{+31.1}_{-27.5}$. The detailed analysis framework developed will serve for the analysis of the overall Run 2 data and could allow extracting a preliminary $t\bar{t}HH$ signal. This work will be carried on with the Run 3 and at the HL-LHC.

Contents

1 Introduction

This note describes a search, performed for the first time with data at the LHC, for the production of a top quark-antiquark pair associated to a pair of Higgs bosons, using the 2017 dataset in CMS. In order to optimize both the signal extraction while keeping as much as possible of the produced events, this analysis considers the semi-leptonic (lepton + jets) decay of the top quark-antiquark pair and the decay of the double Higgs bosons into two bottom quark-antiquark pairs.

In the semi-leptonic (SL) channel, one of the W bosons decays to an electron or a muon and the corresponding neutrino, while the other W boson decays into two quarks. When the two Higgs boson decay both to bottom quarks, this produces the final state $l\nu q\bar{q}b\bar{b}b\bar{b}b\bar{b}$, where l refers to either an electron or a muon, q is a light flavor jet, and b is a jet from a bottom quark. Therefore, ideally at leading order, SL signal events would therefore contain eight relatively high p_{T} jets, at least six of which are b-tagged. However because the Level-1 trigger requirements, the detector acceptance, the possible merging of jets, the b-tagging efficiency, the first stage of the selection in this analysis requests only 4 or more jets and 3 or more b-tagged jets. This optimized the overall analysis sensitivity. The present study thus starts with the same event selection as the one used for the 2017 search for the top pair decaying semileptonically ($\mathrm{t\bar{t}H(b\bar{b})}$). Furthermore, the $\mathrm{t\bar{t}HH}$ (4b's) analysis is guided by the $\mathrm{t\bar{t}H(b\bar{b})}$ analysis strategy [1]. The multivariate classifier based on the deep neural network (DNN) strategy developed for the $\mathrm{t\bar{t}H}$ analysis with similar decays for the tops and the Higgs boson, is further optimized for the $\mathrm{t\bar{t}HH}$ search. All the improvements performed in the 2017 $\mathrm{t\bar{t}H}$ analysis with respect to the one done in 2016 are included here (e.g. a better parton-shower uncertainty modelling based on event weights allowing shape variations; the improved b-tagging performance of the DeepCSV algorithm, leading to approximately 5% higher b-tagging efficiency compared to the previously used CSVv2 algorithm together of course with the upgraded pixel detector). New aspects specific to the $\mathrm{t\bar{t}HH}$ search have been included in the Fit procedure.

The dominant background contribution is QCD top pair+jets production, including all the corresponding $\mathrm{t\bar{t}}$ + jets cases (jets meaning light quark jets or b or c jets) where one or more of the jets is mistagged, and where additional b or c quarks can arise from QCD radiation or loop-induced QCD processes. In addition to the $\mathrm{t\bar{t}}$ + bb background here a new case has to be taken into account, namely the $\mathrm{t\bar{t}}$ +4 b's. It remains almost irreducible with respect to $\mathrm{t\bar{t}}$ +HH (4 b's) with both processes having 6 b quarks in the final state. This issubject to a dedicated study in another Note [2].

Smaller background contributions come from WW+ jets, ZZ + jets, single-top quark, $\mathrm{t\bar{t}}$ +ZZ and $\mathrm{t\bar{t}H}$ productions. In addition to the primary background arising from top quark pair production with additional b quarks, this analysis is affected by a combinatorial background due to multiple b-quark jets in the final state, with no unambiguous way of reconstructing the invariant mass peak of the Higgs boson. Therefore, and even if the $\mathrm{t\bar{t}HH}$ signature is cleaner than the $\mathrm{t\bar{t}H}$ (because of the 2 additional b-jets), an optimal sensitivity for this signal extraction, is achieved with multivariate techniques using simultaneously the differential distributions of several experimental variables. In this analysis, we use deep neural networks (DNNs) optimized on MC simulation. But unlike in the $\mathrm{t\bar{t}H}$ analysis we do not complement by a discriminant based on the direct evaluation of the leading-order $t\bar{t}$ +H and $t\bar{t}$ + $b\bar{b}$ matrix elements on an event-by-event basis (matrix element method).

The analysis proceeds by selecting events with one lepton (either an electron or a muon) and a minimum number of jets and b-tagged jets. The retained events are further categorized based on the jet multiplicity and further event information such as b-tag information into sub-samples with varying signal purity and a different background composition. Categories with low signal purity are useful for constraining background estimates and systematic uncertainties, while categories with higher signal purity provide sensitivity to $t\bar{t}$ + HH production. Backgrounds are modelled using Monte-Carlo (MC) simulated samples corrected to account for known theoretical and experimental deficiencies. The analysis strategy is optimized individually in each channel, similar to the strategy developed with the 2017 $t\bar{t}$H dataset [1]. In the SL channel, DNNs are employed to perform a multi-classification of an event as either signal or any of five different $t\bar{t}$ +jets background processes. The events are consequently categorized by the jet multiplicity and the most-probable process according to the DNN classification, and the corresponding DNN classifier output is used as final. The differences with the $t\bar{t}$H analysis are described in details in the Sections 4 to 7.

In Section 2 the Note describes the Physics motivations for studying this process in terms of the Standard and Beyond Standard Models (SM and BSM) pointing especially the case of the Minimal Composite Higgs Models (MCHM) [3]. Section 3 summarizes the preliminary results of an analysis at parton level, based on MadGraph tools and shows the interplay of the $t\bar{t}$HH production with $t\bar{t}$H and HH processes including both gluon fusion and vector boson fusion (VBF). Section 4 presents the data and Monte Carlo samples used for this analysis stressing the triggers that are used. Section 5 summarizes the event selection especially mentioning the main differences with the one used for the $t\bar{t}$H analysis [1]. Section 6 focuses on the analysis strategy. It details the multivariate analysis performed using Deep Neural Network (DNN) tools and gives the final event classification and sensitivity. Section 7 details the systematics uncertainties with the differences with respect to the $t\bar{t}$H case and presents the Fit Model Validation.

The final results are presented in Section 8 and the Note ends with some final remarks especially on the next steps of this analysis and its short and longer terms perspectives.

2 Physics motivations for the $t\bar{t}$HH search within SM and BSM

The plot in Figure 1 shows the series of processes that are produced in pp collisions that involve the production of double Higgs with a cross section that spans from few tens of fb's to one or a few fb's. They allow accessing a new region in the exploration of the Higgs sector.

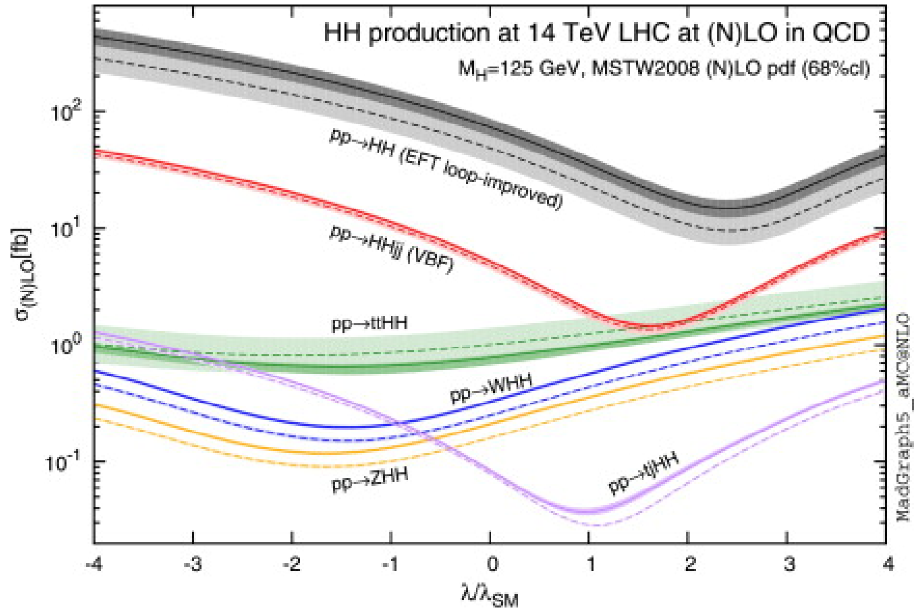

Figure 1. Total cross sections at the LO and NLO in QCD for HH production channels, as a function of the self-interaction coupling λ, taken from Ref [4]. λ is varied for the self-interaction couplings, but the mass of the Higgs boson is fixed to be $m_H = 125$ GeV. The dashed (solid) lines and light-(dark) coloured bands correspond to the LO (NLO) results and to the scale of the PDF uncertainties added linearly. The SM values of the cross-section are obtained at $\lambda/\lambda_{SM} = 1$.

The cross-sections computed at NLO QCD [5] for $t\bar{t}$HH and compared to the ones of VBF (HH) and tjHH are listed in the Table 1.

$\sqrt{s}$(TeV)	ZHH	WHH	VBF HH	$t\bar{t}$HH	tjHH
14	$0.359^{+1.9\%}_{-1.3\%} \pm 1.7\%$	$0.573^{+2.0\%}_{-1.4\%} \pm 1.9\%$	$1.95^{+1.1\%}_{-1.5\%} \pm 2.0\%$	$0.948^{+3.9\%}_{-13.5\%} \pm 3.2\%$	$0.0383^{+5.2\%}_{-3.3\%} \pm 4.7\%$

Table 1. Cross sections computed at NLO QCD for ZHH, WHH, VBF HH, $t\bar{t}$HH and tjHH at 14 TeV center of mass energy.

It is interesting to add the following $t\bar{t}$H and $t\bar{t}$HH production cross-sections [5] listed here below to complete the above Table:

- $\sigma_{t\bar{t}H,13\text{ TeV}}$: 507.1 fb +5.8%-9.2% (QCD scale) $\pm$ 3.6% (PDF + α_s) [5]
- $\sigma_{t\bar{t}H,14\text{ TeV}}$: 613.7 fb +6.0%-9.2% (QCD scale) $\pm$ 3.5% (PDF + α_s) [5]
- $\sigma_{t\bar{t}HH,13\text{ TeV}}$: 0.775 fb +1.5%-4.3% (QCD scale) $\pm$ 3.2% (PDF + α_s) [5]

- $\sigma_{t\bar{t}HH,14\ TeV}$: 0.949 fb +1.7%-4.5% (QCD scale) ± 3.1% (PDF + α_s) [5]

The double Higgs production through the direct process or vector boson fusion are currently under study both in ATLAS and CMS [6, 7]. The aim of our study is to complement these studies by searching for the double Higgs production in association with a top anti-top quark pair.

In the Standard Model, the mechanisms of production at the Leading Order (LO) includes the Yukawa Vertex (80% of the total cross-section) and the trilinear Higgs coupling as shown in Figure 2.

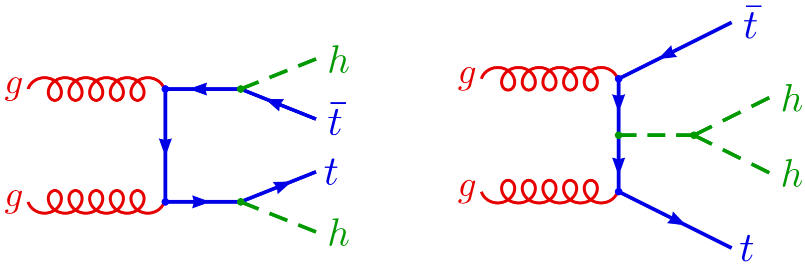

Figure 2. Representative diagrams for the $t\bar{t}$HH process, illustrating the two distinct physical subprocesses: the Yukawa vertex and the Higgs trilinear self-coupling as expected in the SM.

Unlike the $t\bar{t}$H process, the $t\bar{t}$HH production process allows accessing to the triple Higgs coupling at 20% level in the total cross-section. Unlike the double Higgs production the $t\bar{t}$HH does not include interference terms in the access to the triple Higgs coupling. These two facts emphasize the interest of the $t\bar{t}$HH process in the SM, apart from its interest per se.

The $t\bar{t}$HH process plays also a remarkable role when searching for beyond the SM (BSM). Among the theoretical BSM options, this work is especially motivated by the special features of the $t\bar{t}$HH process in the framework of the Minimal Composite Higgs Models (MCHM). Details on the related phenomenological work can be found in the CERN Yellow report on the perspectives for the HL/HE-LHC [8]. A phenomenological work is carried with new inputs in the MCHM studied scenarios and addressing new aspects [3]. We briefly summarize here below the main outcomes of this study of interest for this analysis.

This work considers the production of one or two Higgs bosons in association with a top anti-top pair in the context of Composite Higgs scenarios. The focus is on MCHMs based on the symmetry breaking pattern $SO(5) \rightarrow SO(4)$. In the top sector two possibilities are considered: fermion resonances in the fundamental **5** representation of $SO(5)$ and in the symmetric **14** representation. It is known that there is considerable model-dependence associated with the fermion sector of the MCHM, which is of relevance to this work. In particular, the top sector is expected to play a crucial role given that the top quark couples most strongly to the Higgs boson. The $t\bar{t}$H cross section is measured [9, 10], and is consistent with the SM expectation within the present experimental accuracy, thus still leaving room for deviation from SM.

The $t\bar{t}$HH process has not been yet observed. Such a process is of particular interest in the present class of models, due to the generic prediction of charge 2/3 vector-like

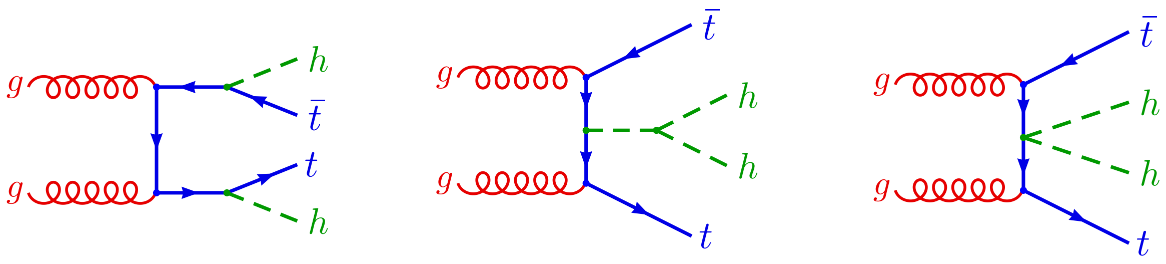

Figure 3. Representative diagrams for the non-resonant $t\bar{t}HH$ process, illustrating the three distinct physical subprocesses: the Yukawa vertex, the Higgs trilinear self-coupling and the "double Higgs" Yukawa vertex arising in composite Higgs scenarios.

"top partners" that can decay in the tH channel, thus leading to the previous final state. Resonance searches focusing on this decay channel have been presented in [11], and combined searches that consider the bW, tZ and tH channels already put constraints on such vector-like resonances [12, 13]

The $t\bar{t}HH$ process has a considerable interest in the non-resonant production. This is important in the regime of heavy resonances and dominates the cross section, being controlled at LO by the MCHM diagrams of Figure 3, which discards the diagrams related to the resonant production of $t\bar{t}HH$ (pair production of resonances that decay in the tH channel). The new diagram on the right of Figure 3 is new in the MCHM, but with present statistics it is negligible. Furthermore the non-resonant $t\bar{t}HH$ process is closely connected to the $t\bar{t}H$ process, but would be expected to display larger deviations from the SM expectation.

All the modifications in the $t\bar{t}H$ production due to Higgs compositeness or mixing with Vector Like Quarks enter only through the top Yukawa coupling, as expressed by the relation:

$$\sigma_{\rm MCHM}(t\bar{t}H) = \left(\frac{y_t}{y_t^{\rm SM}}\right)^2 \sigma_{\rm SM}(t\bar{t}H) \ . \tag{2.1}$$

Thus there is no modification on kinematical distributions with respect to the SM; only the total rates are expected to differ with SM and also between $\rm MCHM_5$ and $\rm MCHM_{14}$. Indeed, in the $\rm MCHM_5$ case, cross section will always be lower than the SM one, while in $\rm MCHM_{14}$, the rate can be either lower or higher than the SM. Thus this is a way already to disregard the $\rm MCHM_5$ or not. These effects also translate to the non resonant $t\bar{t}HH$ leading to even bigger modifications when compared to the SM rates. If resonances play an important role, the $t\bar{t}HH$ cross sections get even higher than the SM in both models.

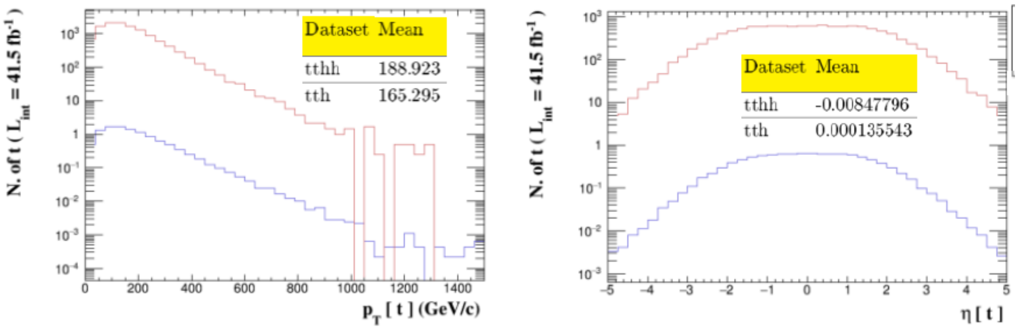

Figure 4. Transverse momentum (p_{T}) and pseudorapidity (η) of the top-quarks produced in $t\bar{t}$H (red line) and $t\bar{t}$HH (blue line) production processes.

3 Study of $t\bar{t}$HH at parton level and interplay with $t\bar{t}$H and HH production processes

An exploratory study has been performed on the $t\bar{t}$HH production process using Madgraph tools. The aim is a preliminary study of this production process at the parton level as well as of the interplay of $t\bar{t}$HH with $t\bar{t}$H and HH processes.

In all three processes the Higgs boson(s) are decaying into b-quark pair thus an emphasis in this study is on the b-quarks their similarities and differences between the three cases. In the Madgraph based generation level considered here, all Higgs are decayed into b-quark pairs, the tops are decayed into Wb and the W is not decayed in the first part of this study. A total of 50,000 events are generated for each process and normalized to 41.5 fb^{-1} luminosity and with cross-sections reweighted to the current published values [5]. Thus for the 2017 data corresponding luminosity a total of 10.9 $t\bar{t}$HH events, 12,256 $t\bar{t}$H events and 492 HH events are expected. For the overall Run 2 (about 140 fb^{-1}) this will translates into 36.7 $t\bar{t}$HH, 41,345 $t\bar{t}$H and 1,660 HH events in total expected.

Several plots are shown here stressing some characteristics of the Higgses and tops and overall jettiness of these different types of events: Figure 4 shows the transverse momentum (p_{T}) and the pseudorapidity (η) of the top-quarks produced in $t\bar{t}$H and $t\bar{t}$HH production processes. There are some small difference between the mean p_{T} values between the tops as produced in $t\bar{t}$HH with respect to those produced in $t\bar{t}$H; in the $t\bar{t}$HH case the mean p_{T} value is slightly larger than the one in $t\bar{t}$HH. The η distributions indicate that the top quarks produced in $t\bar{t}$HH are slightly more central than the tops produced in $t\bar{t}$H (as expected because of their larger p_{T}). Figure 5 shows the transverse momentum (p_{T}) and the pseudorapidity (η) of the b-quarks produced both in the Higgs and the top decays, going from the b-quark with the highest momentum to the one with the second and third lowest momentum. The mean p_{T} of each b-quark produced in $t\bar{t}$HH (4b's)is higher than the ones of the b-quark produced in $t\bar{t}$H (2b's) and HH(4b's). Two additional b-quarks are produced in $t\bar{t}$HH with a lower p_{T} and consequently a larger spread in pseudorapidity. Figure 6 shows the transverse momentum (p_{T}) and the pseudorapidity (η) of the b-quarks produced from the Higgs and top decays but separating

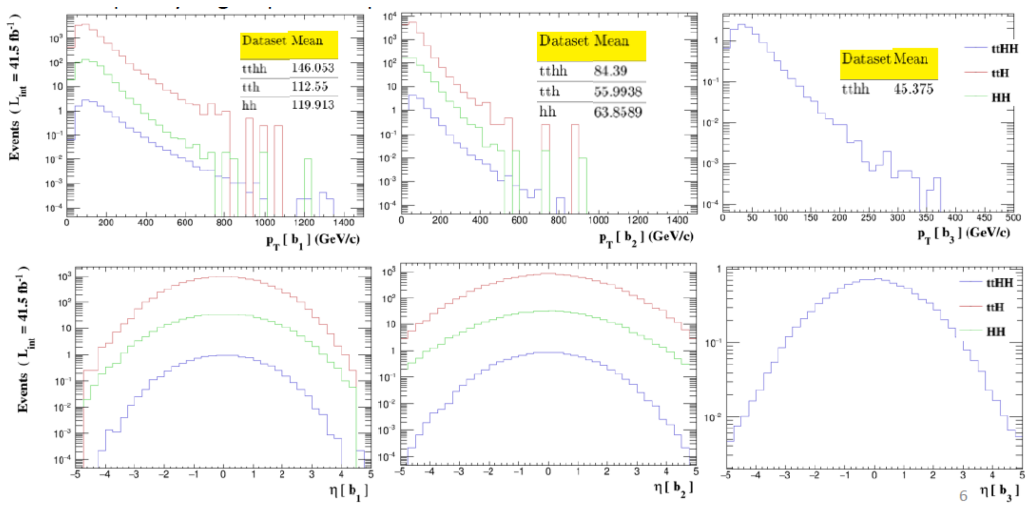

Figure 5. Transverse momentum (p_T) (top distributions) and pseudorapidity (η) (bottom distributions) of the b-quarks produced in t$\bar{\mathrm{t}}$H (red line), t$\bar{\mathrm{t}}$HH (blue line) and HH (green line) production processes. It includes the b-quarks from the top and from the Higgs decays.

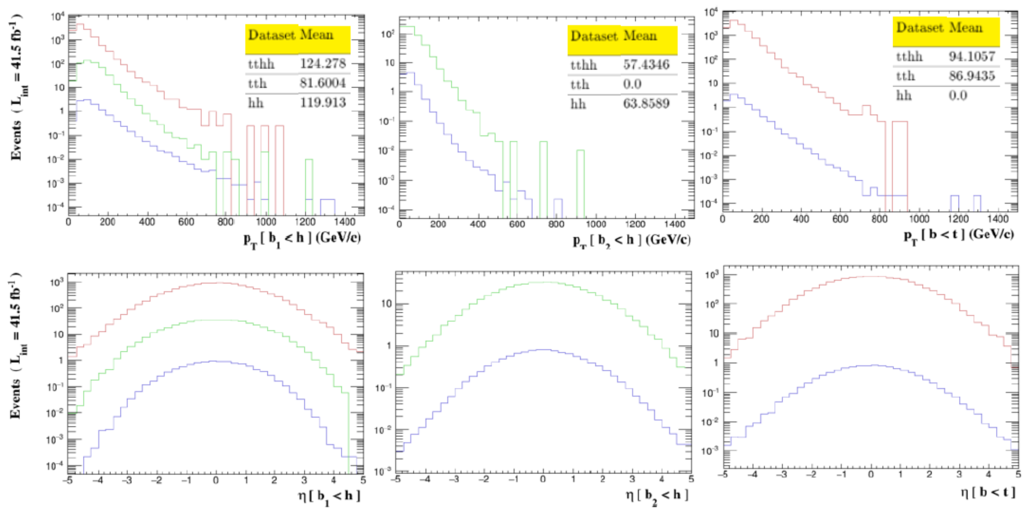

Figure 6. Transverse momentum (p_T) (top distributions) and pseudorapidity (η) (bottom distributions) of the highest and second highest p_T b-quarks produced in the Higgs decays of t$\bar{\mathrm{t}}$H (red line), t$\bar{\mathrm{t}}$HH (blue line) and HH (green line) production processes are shown in the left and middle plots. The corresponding plots for the b-quarks from the top decays are on left.

those coming from the Higgs from those coming from the top and going from the b-quark with the highest momentum to the one with the second and third highest momentum. The features are similar to the ones of Figure 5; in addition, the mean p_T of the b-quarks produced in the top decay are smaller than the highest p_T of the b-quarks produced in the Higgs decay. Figure 7 shows the scalar sum (H_T) of the transverse energy of all the final-state jets. There is no hadronization here, jets are made of individual quarks only.

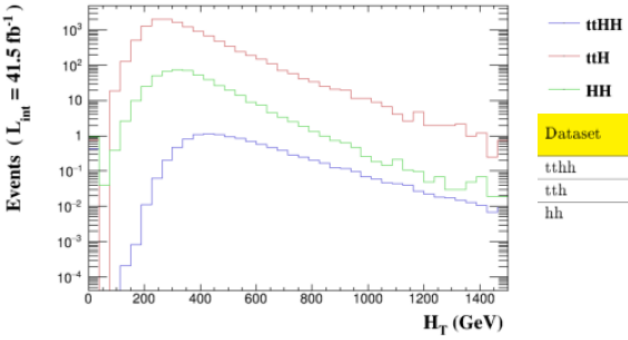

Dataset	Integral	Entries per event	Mean
tthh	10.9	1.0	529.599
tth	12256	1.0	336.473
hh	492	1.0	365.964

Figure 7. Scalar Sum (H_T) distribution for the $t\bar{t}$H (red), HH (green) and $t\bar{t}$HH (blue) processes.

There are only b-quarks as the W is not decayed. As expected and as reflected in the Figure 7, the $t\bar{t}$HH process has the highest jet activity. Table 2 summarizes the tests performed on the effect of selection cuts on the main characteristics of the signature of these events, at the parton level. For this study the W's are decayed. One of the W is decayed into 2 quarks whereas the other one is decayed into a lepton (electron or muon) and the corresponding neutrinos. This is because in this present analysis we only consider the semi-leptonic decay of the top-paires. The cut on the transverse momentum (p_{T}) of the electron resp. the muon is of 30 GeV resp. 29 GeV, the pseudorapidity (η) of the jets and leptons is $\pm$ 2.4 and the cut on the total transverse energy if set at 20 GeV. A test in varying the cut on the p_{T} of the jets from 20 to 30 GeV show some effect but the Level 1 trigger condition imposed to stay at a minimum value of 30 GeV. From this preliminary study, at the level of MadGraph generator and that includes a comparison between the $t\bar{t}$HH, $t\bar{t}$H and HH processes with a special emphasis on the b-quarks, the main observations are:

- The $t\bar{t}$HH events have more jet activity as expected.
- The highest p_{T} b-quark coming from the Higgs has a higher p_{T} in $t\bar{t}$HH process than in $t\bar{t}$H or HH processes.
- The second highest p_{T} b-quark coming from the Higgs has a lower p_{T} and higher spread in pseudorapidity in $t\bar{t}$HH process when compared to the HH process.
- The cuts on jet p_{T} and η reject more events than the other considered cuts; The process $t\bar{t}$HH has a percentage of rejection of the same order than the one of $t\bar{t}$H and HH processes.

This study gives a first hint in this new process we are searching for and its interplay with the two other complementary processes: $t\bar{t}$H and HH production.

	Events Accepted ttHH	ttH	HH
ETA (jets)	71%	67%	71%
PT(jets)>30	33%	30%	54%
PT(b-jets only)>30	51%	58%	54%
ETA (leptons)	95%	92%	-
PT (leptons)	77%	73%	-
MET	80%	90%	-
ETA(jets)&&PT(jets)>20	49% (58%)	46% (58%)	59% (59%)
ETA(jets)&&PT(jets)>25	38% (50%)	35% (51%)	50% (50%)
ETA(jets)&&PT(jets)>30	30% (42%)	24% (44%)	42% (42%)
ETA(jets)&&ETA(leptons)	68%	63%	71%
ETA(jets)&&PT(leptons)	56%	49%	71%
ETA(jets)&&MET	53%	61%	71%

Table 2. Summary of the effect of the different selection cuts (mainly due to the Level 1 trigger conditions) for the three processes. The value in parenthesis shows the % of the remaining events if jets were b-jets only.

4 Data and simulation samples, Trigger, Event reconstruction

The main features of the data and simulation samples, the triggers and the event reconstruction used in this analysis, similar in some way to the one developed for the $t\bar{t}H(b\bar{b})$ search [1, 14] are reviewed, stressing the main differences.

4.1 Data and simulation samples

The data samples are those corresponding to the semi-leptonic case only in [1, 14]. These data sets collected during the 2017 LHC Run at 13 TeV are listed in the Table 3 derived directly from Table 1 of [14]. They are provided by the single lepton Level 1 trigger stream.

From these data sets, certified runs are selected by applying the certified good-run lists as given in [15]. The total integrated luminosity corresponds to L = 41.5 fb^{-1}. The

Sample	Run Range
`/SingleElectron/Run2017B-31Mar2018-v1`	297046–299329
`/SingleElectron/Run2017C-31Mar2018-v1`	299368–302029
`/SingleElectron/Run2017D-31Mar2018-v1`	302030–303434
`/SingleElectron/Run2017E-31Mar2018-v1`	303824–304797
`/SingleElectron/Run2017F-31Mar2018-v1`	305040–306462
`/SingleMuon/Run2017B-31Mar2018-v1`	297046–299329
`/SingleMuon/Run2017C-31Mar2018-v1`	299368–302029
`/SingleMuon/Run2017D-31Mar2018-v1`	302030–303434
`/SingleMuon/Run2017E-31Mar2018-v1`	303824–304797
`/SingleMuon/Run2017F-31Mar2018-v1`	305040–306462

Table 3. Collision data samples used in the analysis.

signal and background events are modeled using MC event samples from the "RunI130 IFall17" MC campaign. The main difference here is of course the $t\bar{t}HH$ data that are sprecially simulated within the Standard Model framework for this analysis. The samples are listed in Table 4 (both MC simulated signal and backgrounds). It has been also requested the production of a sample of 10 M $t\bar{t}ZZ$ simulated data (still to be done). This will be indeed important for the extension of this analysis to the overall Run 2 and after.

The events are generated at next-to-leading order of perturbation theory (NLO) with POWHEG (v. 2) [16] or MADGRAPH5 aMC@NLO (v.2.4.2) [17], or at leading order (LO) with PYTHIA, depending on the process. The value of the Higgs boson mass is assumed to be 125 GeV, while the top quark mass value is set to 172.5 GeV.

The proton structure is described by the parton distribution functions (PDF) NNPDF3.1 [18]. Parton showering and hadronization are simulated with PYTHIA (v. 8.230) [19] and the parameters for the underlying event description correspond to the CP5 tune derived in Ref. [20] based on the work described in Ref. [21] for all signal and background processes. In case of the POWHEG sample the damping parameter (hdamp) has been turned on with a value hdamp = 237.9 GeV. For comparison with the observed distributions, the events in the simulated samples are normalized to the same integrated luminosity of the data sample, according to their predicted cross sections.

All samples are reconstructed with the same CMSSW version 94X as the data samples listed above. The pileup (PU) distribution in all MC samples is reweighted individually, using the standard procedure in CMS, so that the MC PU distribution matches the one expected for data.

The $t\bar{t}$ background samples are listed in Table 4; as in [1] we separate $t\bar{t}$ events into different classes based on the flavor of the additional jets that do not come from the top quark decays in the event. The flavour of those additional jets is determined using the CMS "GenHFHadronMatcher" tool. This tool identifies heavy-flavor (bottom, charm) jets at generator level and finds originating partons to which they correspond. We consider generator-level jets with $p_T > 20$ GeV and abs(η) < 2.4. Based on their flavour, we distinguish:

- $t\bar{t} + b\bar{b}$: event has at least two extra bottom jets, each of which originates from one or more overlapping b hadrons.
- $t\bar{t} + b$: event has only one extra bottom jet which originates from a single b hadron.
- $t\bar{t} + 2b$: event has only one extra bottom jet which originates from two or more overlapping b hadrons.
- $t\bar{t} + c\bar{c}$: event has at least one extra charm jet which originates from one or more overlapping c hadrons.
- $t\bar{t}$ + LF[1]: event does not belong to any of the above classes.

This study takes into account only the $t\bar{t}$ + jets background which is by far the dominant one because of the very small signal we are looking for.

A special case is the contribution of the $t\bar{t}$ + 4b's component of this background. A dedicated work and analysis Note is underway to estimate as precisely as possible this background and the current status is shown in [2]. The last ttbb_Powheg_Openloops simulated file (see Table 4) is especially used for this study. Note that the smaller backgrounds as those taken into account for the $t\bar{t}$H analysis (W, Z+jets, ttW, ttZ , single top, Diboson) are not considered at this stage in this analysis because still too low statistics.

4.2 Trigger

This analysis considers only the semi-leptonic decay of the top pair thus only of interest here are the single lepton channels. The events are therefore selected based on single lepton Level-1 triggers, which require either one electron or one muon. This

[1]Light Flavor

Sample	MiniAOD events	Selected events
/TTHHTo4b_5f_LO_TuneCP5_13TeV_madgraph_pythia8/ RunIIFall17MiniAODv2-PU2017_12Apr2018_94X_mc2017_realistic_v14-v1/	9,800,000	781,129
/ttHTobb_M125_TuneCP5_13TeV-powheg-pythia8/ RunIIFall17MiniAODv2-PU2017_12Apr2018_new_pmx_94X_mc2017_realistic_v14-v1/	8,000,000	239,246
/TTToSemiLeptonic_TuneCP5_PSweights_13TeV-powheg-pythia8/ RunIIFall17MiniAODv2-PU2017_12Apr2018_94X_mc2017_realistic_v14-v2/	110,014,744	584,123
/TTToSemiLeptonic_TuneCP5_13TeV-powheg-pythia8/ RunIIFall17MiniAODv2-PU2017_12Apr2018_new_pmx_94X_mc2017_realistic_v14-v1/	43,732,445	232,264
/TTbb_Powheg_Openloops/asaibel-RunIIFall17MiniAODv2-PU2017_12Apr2018_new_pmx_94X_mc2017_realistic_v14-v1-18783c0a07109245951450a1a4f55409/	5,311,500	212,226

Table 4. Signal and Background Simulation samples used in the analysis.

translates at the HLT into the samples of events contained in the HLT files listed in Table 5. The single-lepton trigger performance in MC simulation has been adjusted based on the performance in data. The trigger efficiency in data and MC are evaluated, and a scale factor (SF), which is the ratio of efficiency in data to that in MC, is applied to MC events in single-electron and single-muon event selection.

Channel	Trigger Name	Run2017 Era
μ	`HLT_IsoMu24_eta2p1_v*`	B–D
	`HLT_IsoMu27_v*`	B–F
e	`HLT_Ele35_WPTight_Gsf_v*`	B–F
	`HLT_Ele28_eta2p1_WPTight_Gsf_HT150_v*`	B–F

Table 5. List of the triggers used in the single-lepton channels.

4.3 Event reconstruction

The software used for ntupling, baseline selection and also selecting the single lepton events are the same used in the $t\bar{t}H(b\bar{b})$ analysis [1, 14]. The MC simulation and data samples are the same and a new $t\bar{t}HH$ MC simulation sample was requested in the same conditions.

The analysis is performed with the CMSSW_9_4_10 version and the global tags used are listed in Table 6, and are used in order to obtain the detector and calibration conditions.

data	94X_dataRun2_v6
MC	94X_mc2017_realistic_v14

Table 6. Global tags used for data and simulation.

Event cleaning is performed by requiring that data and MC events must contain at least one primary vertex (PV) passing the selection, with additional event cleaning using missing transverse energy (MET) filters:

- the number of degrees of freedom used to find the PV must be larger than 4,
- the absolute value of the z-coordinate of the PV must be smaller than 24 cm,
- the absolute value of the ρ-coordinate of the PV must be smaller than 2 cm,
- the PV must not be identified as fake.

Effects from additional pp interactions in the same bunch crossings (PU) are modelled in simulation by adding simulated minimum-bias events to all simulated processes. The PU present in the MC samples does not exactly describe the PU in data. The differences in the distribution of reconstructed primary vertices in MC is corrected by reweighting simulated events to match the PU distribution in data.

Electrons and muons are classified into three types. One definition is designated for the single lepton channel while the other two define leading and sub-leading leptons in the di-lepton channel. The latter is also applied in the semileptonic channel in order to veto extra leptons.

Both lepton candidates are required to pass the cuts on the kinematic variables of p_{T} and η and they have to be sufficiently isolated from nearby jet activity, following the respective relative isolation definition for muons and electrons within a cone of $\Delta\mathrm{R} = 0.4$ for muons and 0.3 for electrons (see [14]). Tables 7 and 8 summarize the muon and electron identification requirements.

	muon ID for single muon channel	leading muon ID for dilepton channel	sub-leading muon ID for dilepton channel
p_{T} [GeV] $>$	29	25	15
$\lvert\eta\rvert <$	2.4	2.4	2.4
$\mathrm{Iso}^{\mu}/p_{\mathrm{T}} <$	0.15	0.25	0.25

Table 7. Summary of muon identification requirements.

	electron ID for single electron channel	leading electron ID for dilepton channel	sub-leading electron ID for dilepton channel
p_{T} [GeV] $>$	30	25	15
$\lvert\eta\rvert <$	2.4	2.4	2.4
$\mathrm{Iso}^{e}/p_{\mathrm{T}} <$	0.06	0.06	0.06

Table 8. Summary of electron identification requirements.

Dedicated scale factors are applied to the MC events in order to improve the agreement with the data, following the recommendations of the EGamma POG [22] for electrons and Muon POG [23] for muons.

Jets are reconstructed with the particle flow algorithm based on reconstructed particle candidates clustered with the anti-kt algorithm with cone size of $\Delta R = 0.4$ (AK4).

The tracks of the particles in the cluster which are associated with non-primary vertices are subtracted to mitigate the impact of pile-up collisions (CHS[2]).

First, in order to increase purity, standard selection criteria ('Jet ID') [24] are applied.

To suppress jets originating from pileup events, loose pileup jet removal is applied following the recommendations by the JME POG [25]. In addition, if any charged lepton passing the selection criteria described above is found within the distance of 0.4 in $\eta - \phi$ space from a jet, then the jet is removed from the analysis.

Prior to the final cuts on the jet kinematics, the jet energies are calibrated with L1, L2 and L3 scale factors (JEC). L2L3Residual corrections are applied on top to real data while jet energy smearing is performed on MC samples by considering the difference in p_{T} between the reconstructed and its associated generated jet. The deployed JEC corresponds to the set in the global tags listed in Tab. 6 and the JER correction factors are as in [26], following the JME POG recommendations.

The requirements on the jet kinematics are listed in Table 9.

	single-lepton channel	dilepton channel	
	jets	leading 2 jets	further jets
min p_{T} [GeV]	30	30	20
max $\lvert\eta\rvert$	2.4	2.4	2.4

Table 9. Jet kinematic selection requirements.

We use the DeepCSV [27] b-tagging discriminator to identify jets that originate from b-quark decays (referred to as b-tagged jets). Jets are defined to be b-tagged if their b-tagging discriminator is larger than 0.4941 (medium working point). Differences in the b-tagging efficiency and mis-tag rate between data and simulated events are taken into account via weights. The same framework and DeepCSV version used in the $\mathrm{t\bar{t}H(b\bar{b})}$ analysis is used and described in [14].

In addition a L1 prefiring correction is also taken into account by using event weights. No modification from the $\mathrm{t\bar{t}H}$ analysis was done in this respect as well and all distributions are scaled by the appropriate scale factors.

[2]Charged Hadron Subtraction

5 Event selection

The n-tupling program, used to select the semi-leptonic decay for top pairs and double Higgs decay into b-quarks is the same as the one used in the $t\bar{t}H(b\bar{b})$ analysis as shown in Table 10. On top of this selection, events are required to have a missing transverse energy of at least 20 GeV and an extra b tagged jet is required leading to at least 3 b tagged jets with the DeepCSV b-tagging discriminator at the medium working point (DeepCSV > 0.4941).

	SL channel
Number of leptons	1
p_T of leptons (e/μ) [GeV]	$> 30/29$
p_T of additional leptons [GeV]	< 15
$\lvert\eta\rvert$ of leptons	< 2.4
Number of jets	≥ 4
p_T of jets [GeV]	> 30
$\lvert\eta\rvert$ of jets	< 2.4
Number of b tagged jets	≥ 2

Table 10. Baseline event selection criteria in the single-lepton channel.

Process	Total number of selected events
$t\bar{t}$ + LF	360,877
$t\bar{t} + c\bar{c}$	94,235
$t\bar{t}$ + b	58,473
$t\bar{t}$ + 2b	27,875
$t\bar{t} + b\bar{b}$	42,663
Total $t\bar{t}$	584,123
$t\bar{t}H$	239,246
$t\bar{t}HH$	390,663

Table 11. Number of selected events used for fitting (see section 7). The baseline selection of table 10 is applied together with requiring ≥ 3 b-tagged jets.

Tables 11 and 12 show the selected number of events used for the DNN modeling and the fitting steps of the analysis. A higher number of b-tagged jets and a higher DeepCSV b-tagging discriminator value didn't work because of too few events left for this analysis.

Process	Total number of selected events
$t\bar{t} + \mathrm{LF}$	143,490
$t\bar{t} + c\bar{c}$	37,291
$t\bar{t} + b$	23,409
$t\bar{t} + 2b$	11,056
$t\bar{t} + b\bar{b}$	17,018
Total $t\bar{t}$	232,264
$t\bar{t}HH$	390,466

Table 12. Number of selected events used for DNN modeling (see section 6). The baseline selection of table 10 is applied together with requiring ≥ 3 b-tagged jets.

	(≥ 4 jets, ≥ 3 b-tags)
nodes per hidden layer	3×100
loss function	cross-entropy
dropout percentage	0.5
L2 regularization	10^{-5}
batchsize	5000
optimizer	ADAM(10^{-4})
activation function	ELU
last activation	softmax
earlystopping percentage	2%
earlystopping min epochs	50

Table 13. Hyperparameters of the neural network.

6 Analysis strategy

The strategy followed in this analysis is based on Deep Neural Network tools allowing an optimized event classification and analysis sensitivity.

6.1 Deep Neural Networks

The $\mathrm{t\bar{t}H}$ (SL, Higgs to $\mathrm{b\bar{b}}$) analysis [1, 14], based on a Deep Neural Network (DNN) strategy developed for the 2016 analysis [28] with an architecture optimized for the 2017 data, leads to an overall higher sensitivity than a jet and b-tag multiplicity based categorisation. This is why this analysis has chosen to use the 2017 data DNN framework further optimized for this $\mathrm{t\bar{t}HH}$ analysis. Following the event selection described in Section 5, a DNN is used as a classifier in order to separate signal ($\mathrm{t\bar{t}HH}$) events and each of the five $\mathrm{t\bar{t}}$ + jets background processes $\mathrm{t\bar{t}+b\bar{b}}$, $\mathrm{t\bar{t}+2b}$, $\mathrm{t\bar{t}+b}$, $\mathrm{t\bar{t}+c\bar{c}}$, or $\mathrm{t\bar{t}+LF}$. Each of these six categories are implemented as output nodes in the DNN modeling. Thus the DNN is used to categorize events into the most probable process and further construct the final discriminants that will be used for the final fit.

The DNN architecture and implementation did not change from what was described in the $\mathrm{t\bar{t}H}$ analysis [14]. It is implemented in Keras as a feedforward neural network with three hidden layers of 100 nodes each. The cost function that is minimised during the training is the categorical cross entropy. The network architecture is listed in Table 13.

Each of the training samples is further split into a subset "training" for the actual training (60 %) and an independent subset "test" for immediate cross-validation and hyperparameter optimisation (20 %) as well as a further independent subset "validation" (20%), which is used to study the performance of the DNNs.

Table 12 show the selected events to be used for DNN training, and are independent from the events listed in Table 11.

The input variables used by the DNN are listed in Appendix A. These variables are related to kinematic properties of individual objects, event shape and the b tagging discriminant. A first training of the DNN is performed using all the variables listed in Appendix A, but the final model contains only the 20 most important variables ranked by weight. The performance of the model in this last case when compared to the one containing all variables is similar within 1%. Table 14 shows the top 20 variables for this analysis.

H_1	$\Delta\eta_{b,b}^{avg}$
$\Delta R_{lep,b}^{min}$	pt_j^{avg}/E_j^{avg}
$\Sigma_j(d-d_j^{avg})^2$	$m_{b,b}^{min\Delta R}$
$N_b(loose)$	BLR
$pt(jet1)$	d_j^{avg}
d_3	$(m^2)_b^{avg}$
d_b^{avg}	$N_b(medium)$
$\Delta\eta_{j,j}^{avg}$	d_4
H_T^b	BLR^{trans}
H_T	m_b^{avg}

Table 14. Top 20 ranked Input Variables for this analysis, defined in Appendix A.

Different jet categorization was also studied. Unlike the $t\bar{t}H$ analysis, separating events by jet multiplicity gave a worse performance, because of having very few $t\bar{t}HH$ events in categories such as (4 jets, $\geq$ 3 b-tags) or (5 jets, $\geq$ 3 b-tags). On the other hand, categories with higher jet multiplicity have more $t\bar{t}HH$ events, but there is no gain in performance when compared to the category we use, a single ($\geq$ 4 jets, $\geq$ 3 b-tags) category. Different categories containing combination of jet multiplicities also either do not affect performance or lead to a worse performance. A study on changing the event selection by the number of b tags also lead to a decrease in performance because of few events surviving, and the same applies for changing the b tagging working point from medium to tight. The event selection by b tagging was kept the same and the number of b tagged jets passing the lose, medium or tight working points were included in the DNN as input variables. It was also checked the effect of adding $t\bar{t}H$ as an output node in the DNN, but this lead to a drop in performance of about 10% in the $t\bar{t}HH$ node.

Figure 8 shows the final confusion matrix which shows a classification efficiency of 71.6%, which is quite high thanks to the two additional b quarks when compared to $t\bar{t}H(b\bar{b})$. Figure 8 also shows the loss function of this model.

Figure 9 shows the events classified in each output node and events plotted are a sub-sample of the events used during training. These distributions show the difference in shape obtained for the $t\bar{t}HH$ event distribution when compared to the $t\bar{t}$ background. The final discriminants, constructed with this trained DNN model and the bigger sub-sample of events used for the fitting part of the analysis is discussed in the next section.

6.2 Final event classification and sensitivity

After training the DNN model, the events of Table 11 are used for constructing the final discriminant distributions that will be used for fitting. The background nodes are listed in Figure 10. The signal nodes are presented for different cases in Section 7, each of these cases containing different bin widths and/or different set of systematic uncertainties.

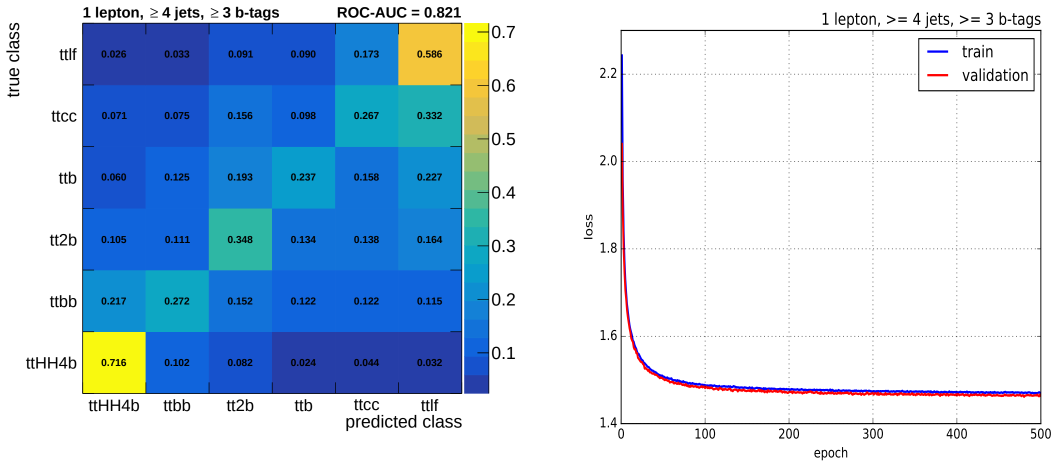

Figure 8. Confusion matrix and loss function for the trained DNN model

The background nodes presented here are the same for all cases and contain all shape systematic uncertainties (see Section 7) added in quadrature.

The binning of these background nodes was chosen to have at least 30 expected background events in each bin. The fit results does not change too much if the number of bins is reduced. Here we choose to keep more bins to retain the distribution shapes which could be useful for the next steps of the analysis (using full Run 2 data) and beyond, but for the current work the shape of the distributions on the background nodes does not influence much the results of the shape analysis presented in Section 7.

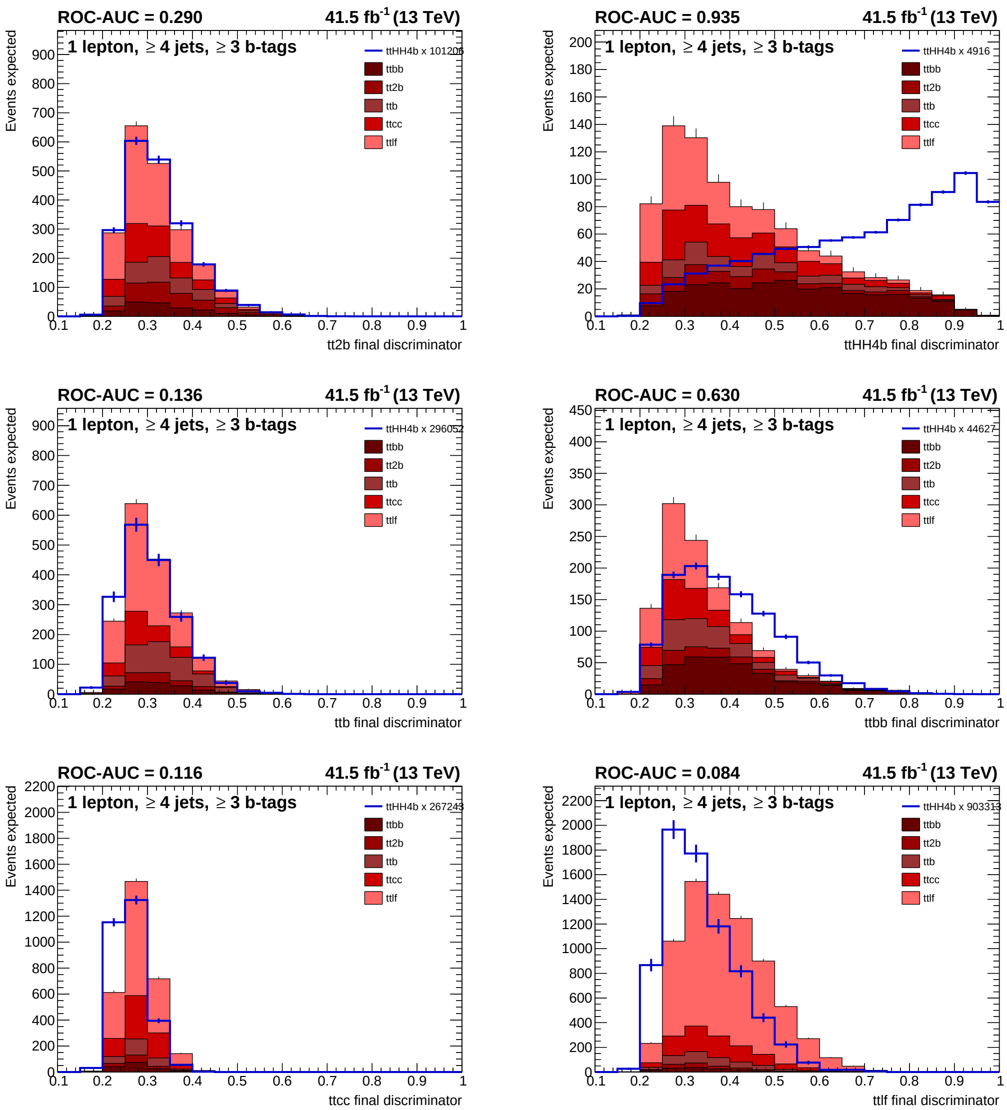

Figure 9. Comparison of the DNN discriminant distributions expected for the signal and background processes, constructed with a subset of 20% of the events listed in Table 12 and normalized to 41.5 fb^{-1} luminosity.

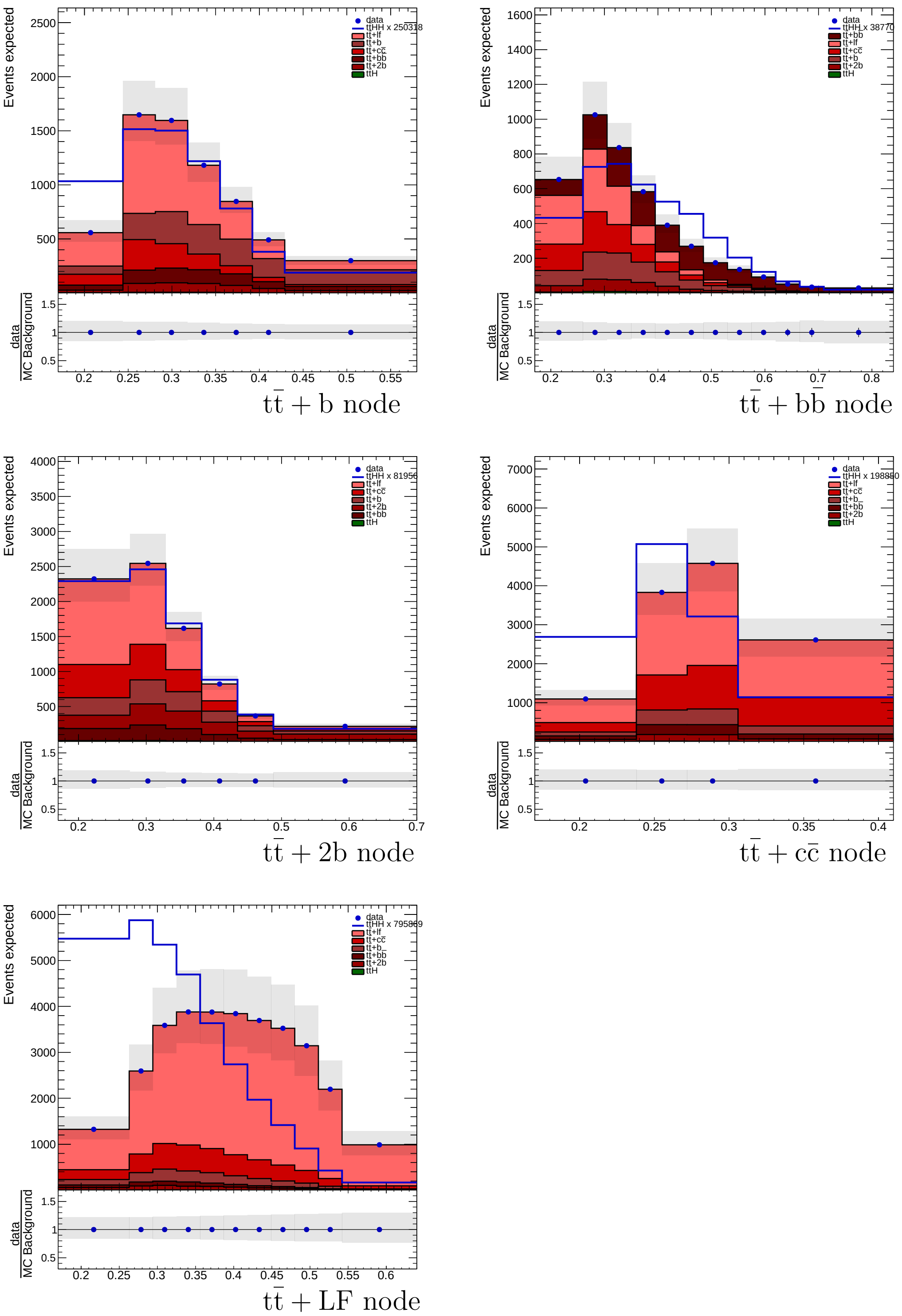

Figure 10. Final discriminant distributions, for all the background nodes, constructed with signal and background processes listed in Table 11 and normalized to 41.5 fb^{-1} luminosity. Data presented here is Asimov data.

7 Systematics uncertainties and Fit Model Validation

After having the trained DNN model and constructing the discriminants with events of Table 11, this section shows how the systematics uncertainties are included in the analysis for the fitting to (Asimov) data. The discriminants used for the fitting part were already presented in Figure 10, showing the common background nodes for the different cases to be presented here. The final discriminators for the signal node will be presented in this section and is different for each studied case.

7.1 `combine` Tool

All fits and statistical analyses are performed with the Higgs combine tool version v8.0.1 in the CMSSW_10_2_13 environment.

7.2 Systematic uncertainties

The systematic effects considered in this analysis of the 2017 dataset are described in Table 15. Each rate systematic was added at the datacard level, while for shape systematics, varied templates with up/down variation are generated. For JER and JES systematics, the full analysis is redone starting from the ntuple creation, and events are fed to the trained DNN for creating the final discriminants. The rate inclusive cross section uncertainties are summarized in Table 16. This is a similar Table of systematics uncertainties than for $\mathrm{t\bar{t}H(b\bar{b})}$ except adding of course $\mathrm{t\bar{t}HH}$ and not including the smaller background processes (see Section 4.1), not yet considered in this analysis because still too low data rate.

Source	Type	Remarks
Integrated luminosity	rate	Signal and all backgrounds
Lepton identification/isolation	shape	Signal and all backgrounds
Trigger efficiency	shape	Signal and all backgrounds
Trigger prefiring correction	rate	Signal and all backgrounds
Pileup	shape	Signal and all backgrounds
Jet energy scale	shape	Signal and all backgrounds
Jet energy resolution	shape	Signal and all backgrounds
b tag hf fraction	shape	Signal and all backgrounds
b tag hf stats (linear)	shape	Signal and all backgrounds
b tag hf stats (quadratic)	shape	Signal and all backgrounds
b tag lf fraction	shape	Signal and all backgrounds
b tag lf stats (linear)	shape	Signal and all backgrounds
b tag lf stats (quadratic)	shape	Signal and all backgrounds
b tag charm (linear)	shape	Signal and all backgrounds
b tag charm (quadratic)	shape	Signal and all backgrounds
Renorm./fact. scales ($t\bar{t}H$)	rate	Scale uncertainty of NLO $t\bar{t}H$ prediction
Renorm./fact. scales ($t\bar{t}$)	rate	Scale uncertainty of NNLO $t\bar{t}$ prediction
Renorm./fact. scales ($t\bar{t}HH$)	rate	Scale uncertainty of NLO $t\bar{t}HH$ prediction
$t\bar{t}+HF$ cross sections	rate	Additional 50% rate uncertainty of $t\bar{t}+HF$ predictions
PDF (gg)	rate	PDF uncertainty for gg initiated processes except $t\bar{t}H$ and $t\bar{t}HH$
PDF (gg $t\bar{t}H$)	rate	PDF uncertainty for $t\bar{t}H$
PDF (gg $t\bar{t}HH$)	rate	PDF uncertainty for $t\bar{t}HH$
PDF shape variations ($t\bar{t}H$, $t\bar{t}HH$, $t\bar{t}$)	shape	Based on the NNPDF replicas, same for $t\bar{t}H$, $t\bar{t}HH$ and additional jet flavours
μ_R scale ($t\bar{t}$)	shape	Renormalisation scale uncertainty of the $t\bar{t}$ ME generator (POWHEG), same for additional jet flavours
μ_F scale ($t\bar{t}$)	shape	Factorisation scale uncertainty of the $t\bar{t}$ ME generator (POWHEG), same for additional jet flavours
PS scale: ISR ($t\bar{t}$)	shape	Initial state radiation uncertainty of the PS (for $t\bar{t}$ events), same for additional jet flavours
PS scale: FSR ($t\bar{t}$)	shape	Final state radiation uncertainty of the PS (for $t\bar{t}$ events), same for additional jet flavours
Bin-by-bin event count	shape	Statistical uncertainty of the signal and background prediction due to the limited sample size

Table 15. Systematic uncertainties considered in this analysis.

Process	PDF			Renorm./fact. scales		
	$gg_{\mathrm{t\bar{t}H}}$	$gg_{\mathrm{t\bar{t}HH}}$	gg	$t\bar{t}$	$t\bar{t}H$	$t\bar{t}HH$
$t\bar{t}H$	3.6%				-9.2%/+5.8%	
$t\bar{t}HH$		3.2%				-4.3%/+1.5%
$t\bar{t}$+jets			4%	-4%/+2%		

Table 16. Inclusive cross section (rate) uncertainties used in the analysis. Note that an extra 50% rate uncertainty is assigned separately to each of the four considered $\mathrm{t\bar{t}}+\mathrm{HF}$ processes.

7.3 Fit Results

The fitting is performed in different cases that differ in the binning of the discriminant histograms and/or in the set of systematics that are included. Each case is presented separately in the following sections and the best case for the present analysis is chosen and presented in Section 8. The background nodes, presented in Figure 10, are the same in all cases and include five of the six discriminators used for the fitting, each including $\mathrm{t\bar{t}HH}$, $\mathrm{t\bar{t}+LF}$, $\mathrm{t\bar{t}+c\bar{c}}$, $\mathrm{t\bar{t}+b\bar{b}}$, $\mathrm{t\bar{t}+2b}$, $\mathrm{t\bar{t}+b}$ and $\mathrm{t\bar{t}H}$. All bins have at least 30 expected background events. The analysis is not too sensitive to the shape of distributions in these background nodes, but they were kept in this analysis. In the full Run 2 analysis this study will be redone. For the signal nodes, each case is treated differently and in the next sections the discriminants are presented.

7.3.1 Case 1

This case considers at least 1 expected background event in each bin of the signal node. Figure 11 shows this choice of binning. The shape systematics are also included in these plots and added in quadrature. Data points are Asimov data. JES systematics are split into the different sources. Each difference JES systematic up/down variation is produced by redoing the ntuples and performing the DNN classification again for each varied template and the final discriminant is then produced.

A fit is performed and results are obtained for the signal strength $\mu = \sigma/\sigma_{SM}$. Summarized in Table 17 are a case with no systematics on the top row and with all systematics on the bottom row. The analysis for this 2017 luminosity is dominated by statistics. This complete systematics framework will be used and indeed more relevant in the future studies involving full Run 2 and the upcoming Run 3 and also High Luminosity LHC (HL LHC). The middle row shows a result excluding the “bin-by-bin statistics” systematics. This exclusion is performed because in a preliminary extrapolation of this result to higher luminosity (see Section 8) using the `combine` tool. This is needed to avoid a conflict at the technical level with this tool.

Impacts and pulls are shown in Figures 12 and 13. These figures show the systematics ranked by impacts and the JES systematics are the highest ranked, as well as being one-sided in $\Delta\mu$ (Δr in the Figure).

No systematics	Best fit (μ)	Observed (Asimov)	$1^{+23.2}_{-17.0}$
	95% CL upper limits on μ	Expected (Median)	49.8
		Expected (68% CL range)	[34.2,73.0]
		Expected (95% CL range)	[24.9,102.6]
All systematics (excluding bin-by-bin statistics)	Best fit (μ)	Observed (Asimov)	$1^{+26.4}_{-20.2}$
	95% CL upper limits on μ	Expected (Median)	58.3
		Expected (68% CL range)	[39.5,87.5]
		Expected (95% CL range)	[28.2,126.7]
All systematics	Best fit (μ)	Observed (Asimov)	$1^{+27.3}_{-21.6}$
	95% CL upper limits on μ	Expected (Median)	61.0
		Expected (68% CL range)	[40.8,90.3]
		Expected (95% CL range)	[29.3,130.9]

Table 17. Fit Results for Case 1

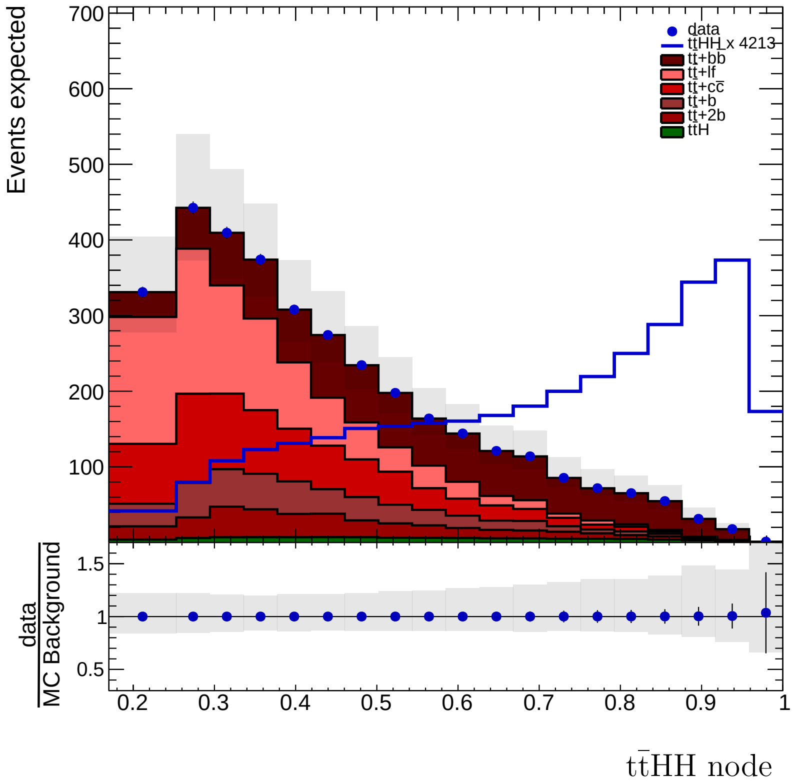

Figure 11. Final discriminant distribution for the signal node, constructed with signal and background processes listed in Table 11 and normalized to 41.5 fb^{-1} luminosity. Data presented here is Asimov data.

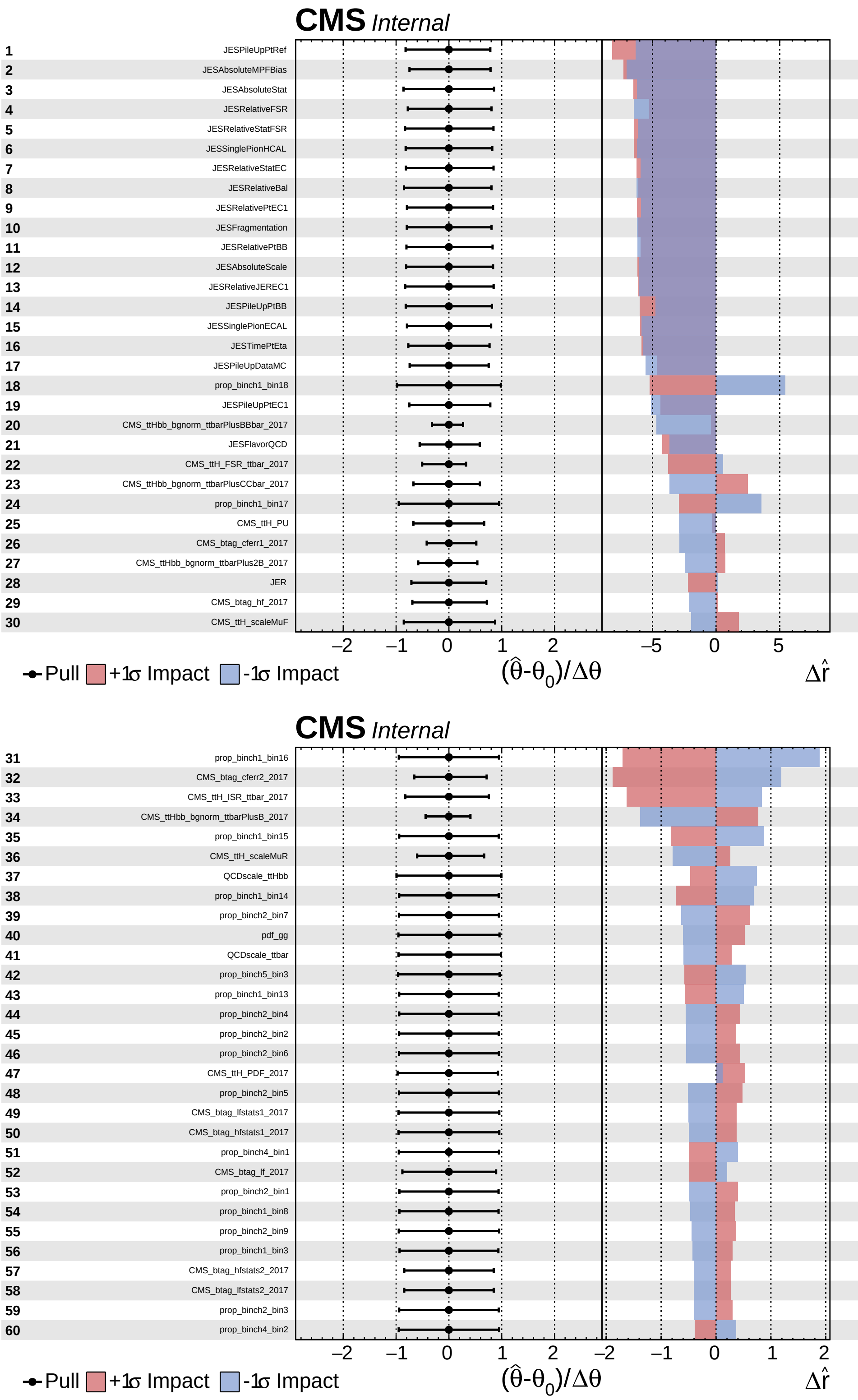

Figure 12. Nuisance parameter pulls and impacts, sorted by the largest impact, obtained from a fit to Asimov data corresponding to the 2017 dataset for the 110 nuisance parameters ranked highest in impact. Continued in Figure 13.

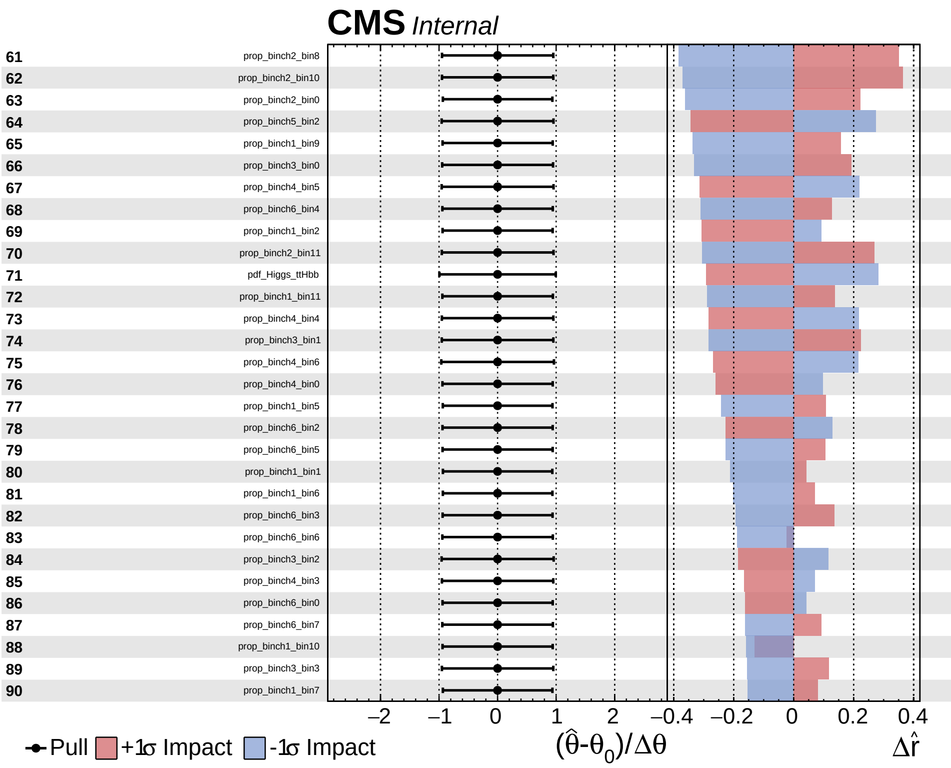

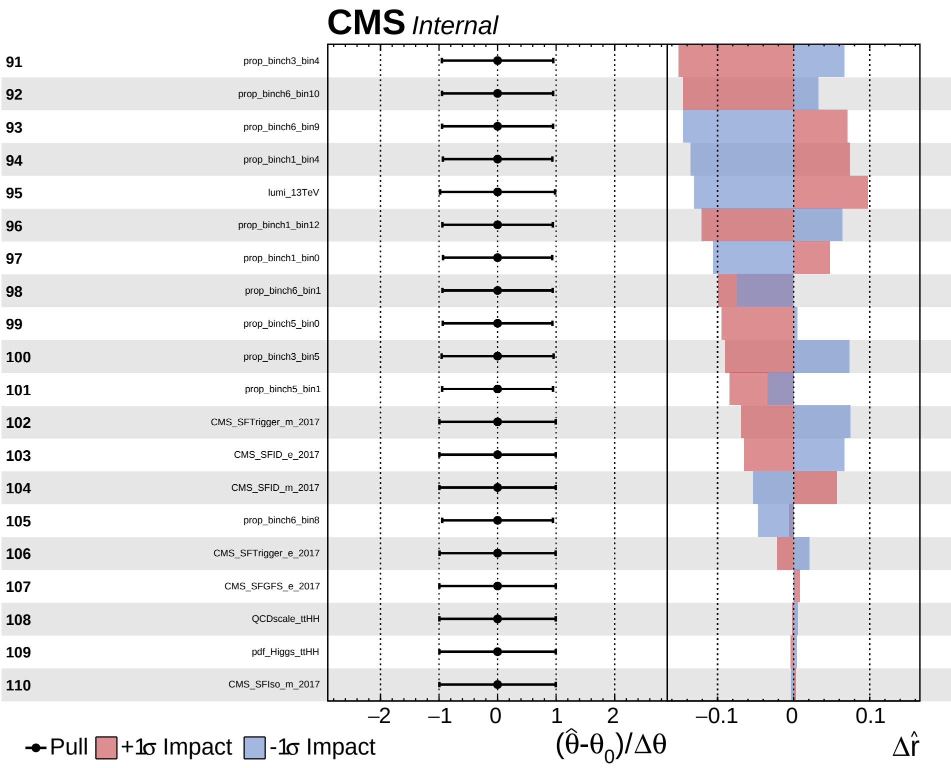

Figure 13. Continued from Figure 12

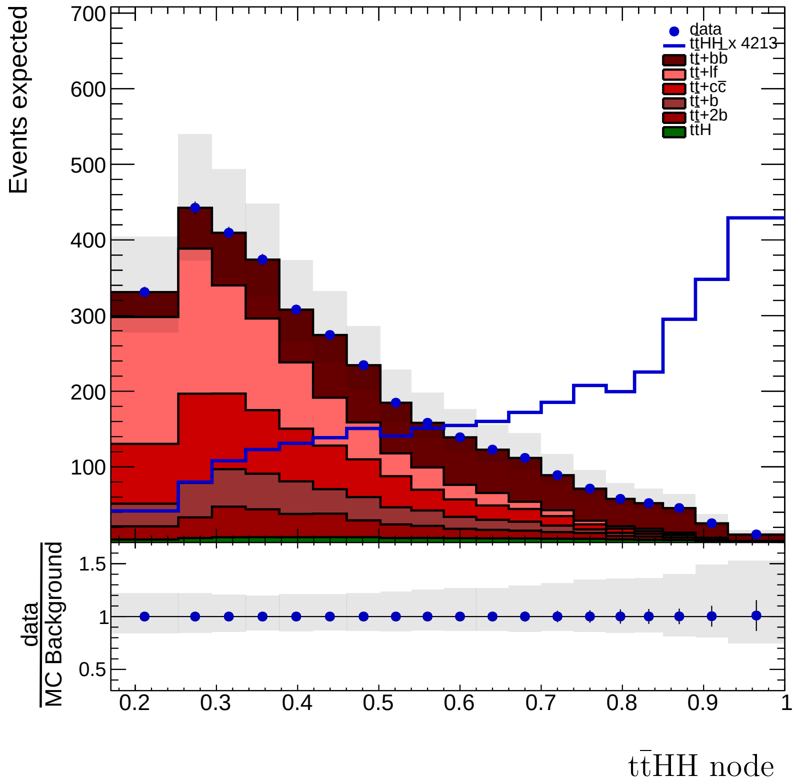

Figure 14. Final discriminant distribution for the signal node, constructed with signal and background processes listed in Table 11 and normalized to 41.5 fb^{-1} luminosity. Data presented here is Asimov data.

7.3.2 Case 2

This case considers at least 10 expected background events in each bin of the signal. Figure 14 shows this choice of binning. The shape systematics are also included in these plots and added in quadrature. Data points is Asimov data. JES systematics are split into the different sources and the varied templated are obtained in the same way explained for Case 1.

A fit is the performed and results are obtained for the signal strength μ and summarized in Table 18 in the same way done for Case 1. Impacts and pulls are shown in Figures 15 and 16. These figures show the systematics ranked by impacts and the JES systematics are the highest ranked, as well as being one-sided in $\Delta\mu$ (Δr in the Figure), similar to Case 1.

No systematics	Best fit (μ)	Observed (Asimov)	$1^{+26.5}_{-23.7}$
	95% CL upper limits on μ	Expected (Median)	54.5
		Expected (68% CL range)	[38.3,78.2]
		Expected (95% CL range)	[28.3,107.9]
All systematics (excluding bin-by-bin statistics)	Best fit (μ)	Observed (Asimov)	$1^{+31.3}_{-29.7}$
	95% CL upper limits on μ	Expected (Median)	65.5
		Expected (68% CL range)	[45.5,95.5]
		Expected (95% CL range)	[33.5,135.6]
All systematics	Best fit (μ)	Observed (Asimov)	$1^{+32.7}_{-31.5}$
	95% CL upper limits on μ	Expected (Median)	67.9
		Expected (68% CL range)	[47.4,99.1]
		Expected (95% CL range)	[35.0,139.8]

Table 18. Asimov Results for Case 2.

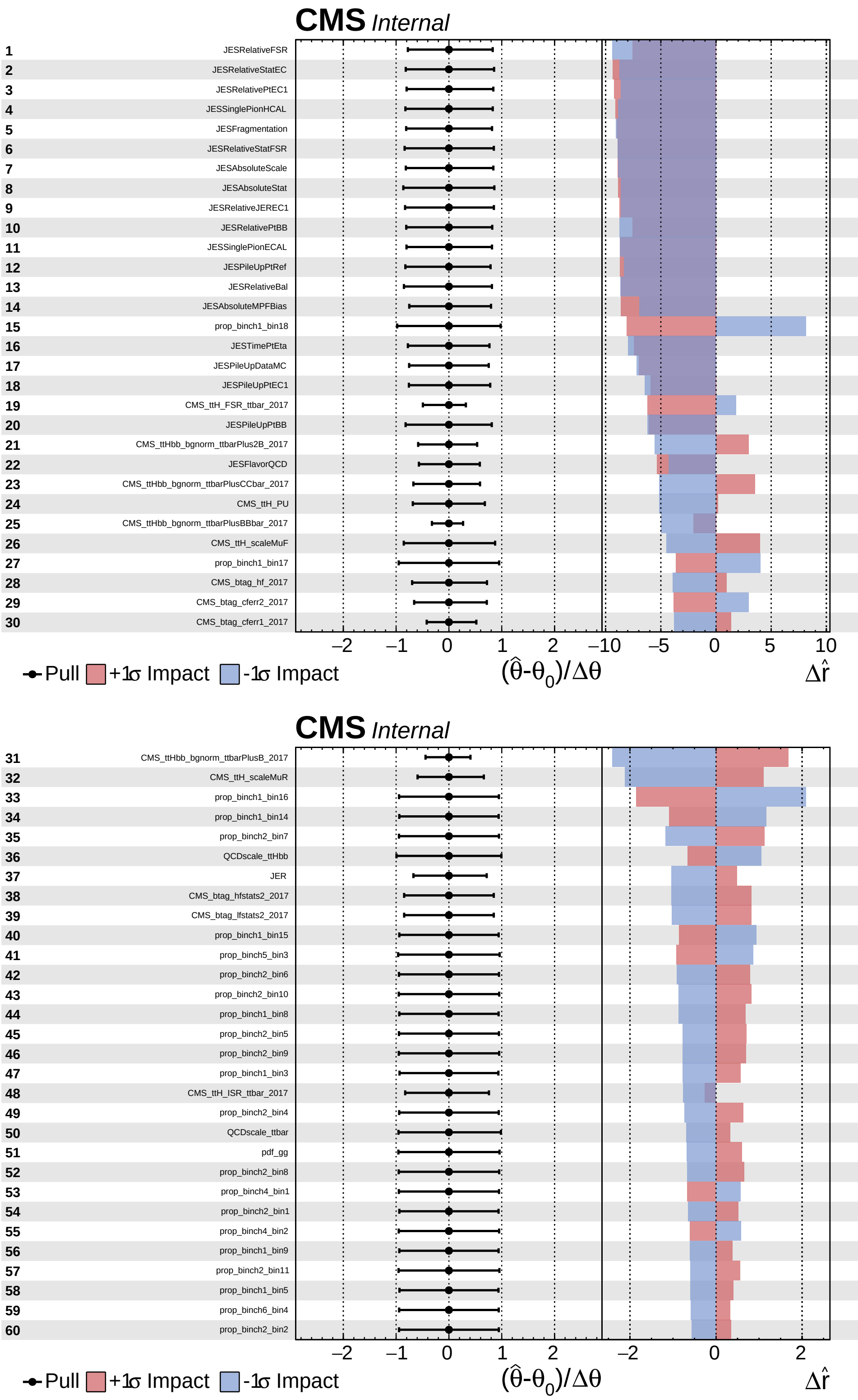

Figure 15. Nuisance parameter pulls and impacts, sorted by the largest impact, obtained from a fit to Asimov data corresponding to the 2017 dataset for the 110 nuisance parameters ranked highest in impact. Continued in Figure 16.

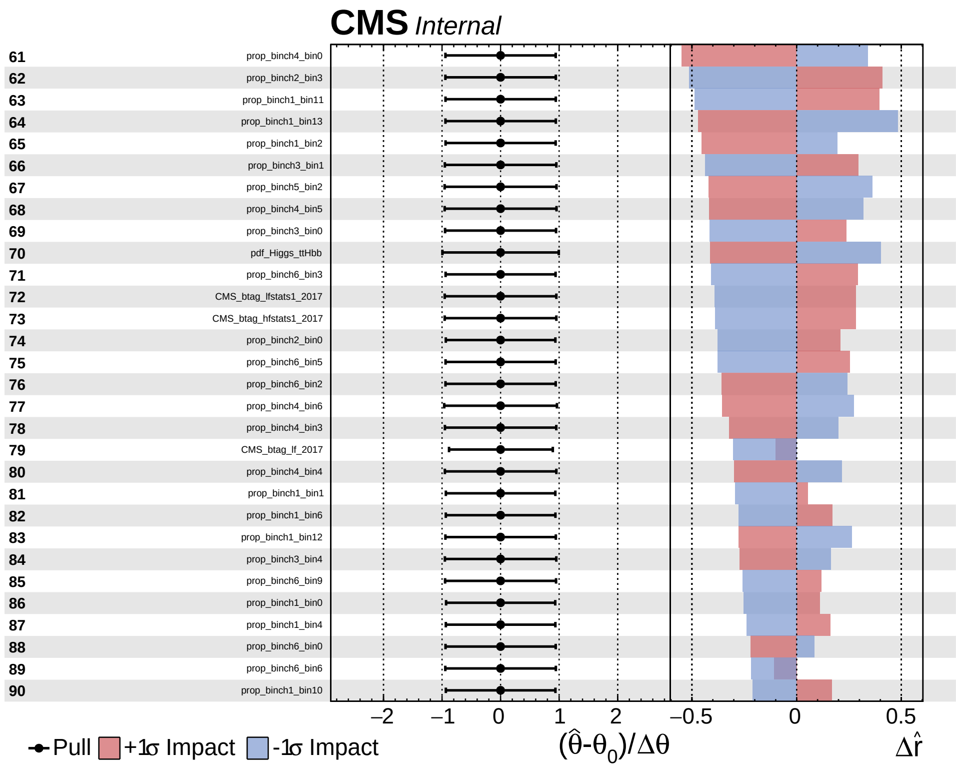

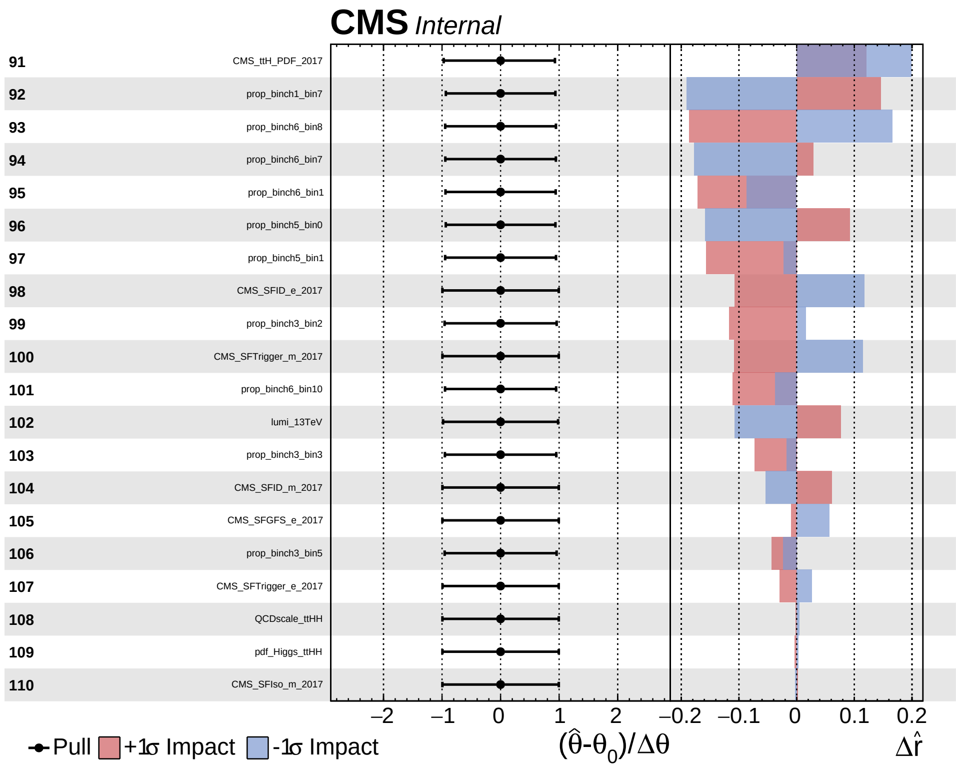

Figure 16. Continued from Figure 15

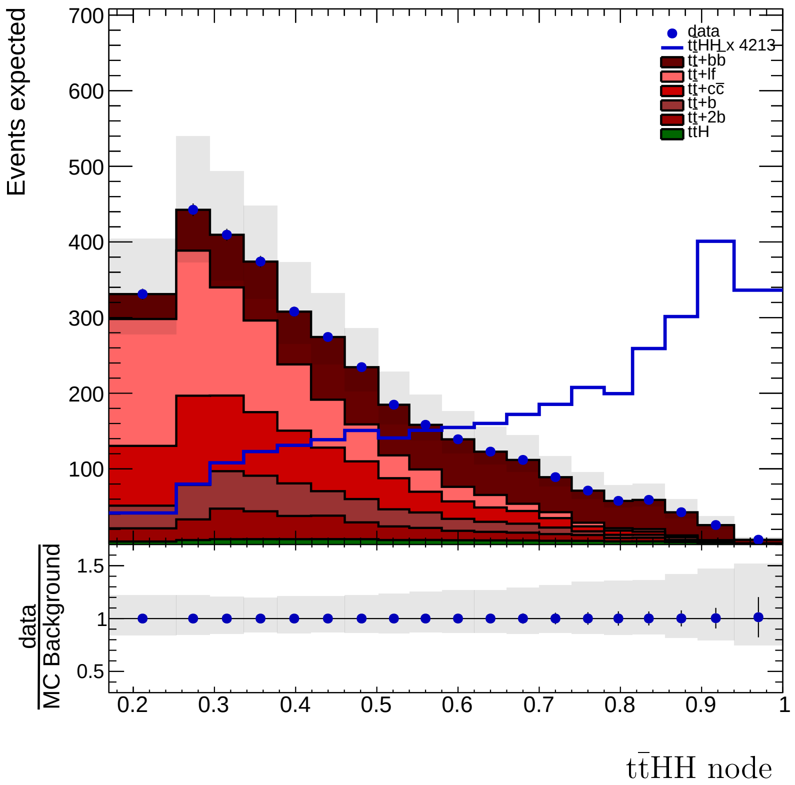

Figure 17. Final discriminant distribution for the signal node, constructed with signal and background processes listed in Table 11 and normalized to 41.5 fb^{-1} luminosity. Data presented here is Asimov data.

7.3.3 Case 3

This case considers at least 6 expected background events in each bin of the signal node, in between Cases 1 and 2. Figure 17 shows this choice of binning. The shape systematics are also included in these plots and added in quadrature. Data points is Asimov data. JES systematics are split into the different sources and the varied templates are obtained in the same way explained for Cases 1 and 2.

A fit is the performed and results are obtained for the signal strength μ and summarized in Table 19 in the same way done for Cases 1 and 2. Impacts and pulls are shown in Figures 18 and 19. These figures show the systematics ranked by impacts and the JES systematics are the highest ranked, as well as being one-sided in $\Delta\mu$ (Δr in the Figure), similar to Cases 1 and 2.

No systematics	Best fit (μ)	Observed (Asimov)	$1^{+25.6}_{-22.4}$
	95% CL upper limits on μ	Expected (Median)	53.3
		Expected (68% CL range)	[37.1,76.6]
		Expected (95% CL range)	[27.5,106.3]
All systematics (excluding bin-by-bin statistics)	Best fit (μ)	Observed (Asimov)	$1^{+29.8}_{-27.5}$
	95% CL upper limits on μ	Expected (Median)	63.0
		Expected (68% CL range)	[43.6,92.9]
		Expected (95% CL range)	[32.0,132.2]
All systematics	Best fit (μ)	Observed (Asimov)	$1^{+31.1}_{-29.1}$
	95% CL upper limits on μ	Expected (Median)	65.5
		Expected (68% CL range)	[45.4,96.1]
		Expected (95% CL range)	[33.3,136.7]

Table 19. Asimov Results for Case 3

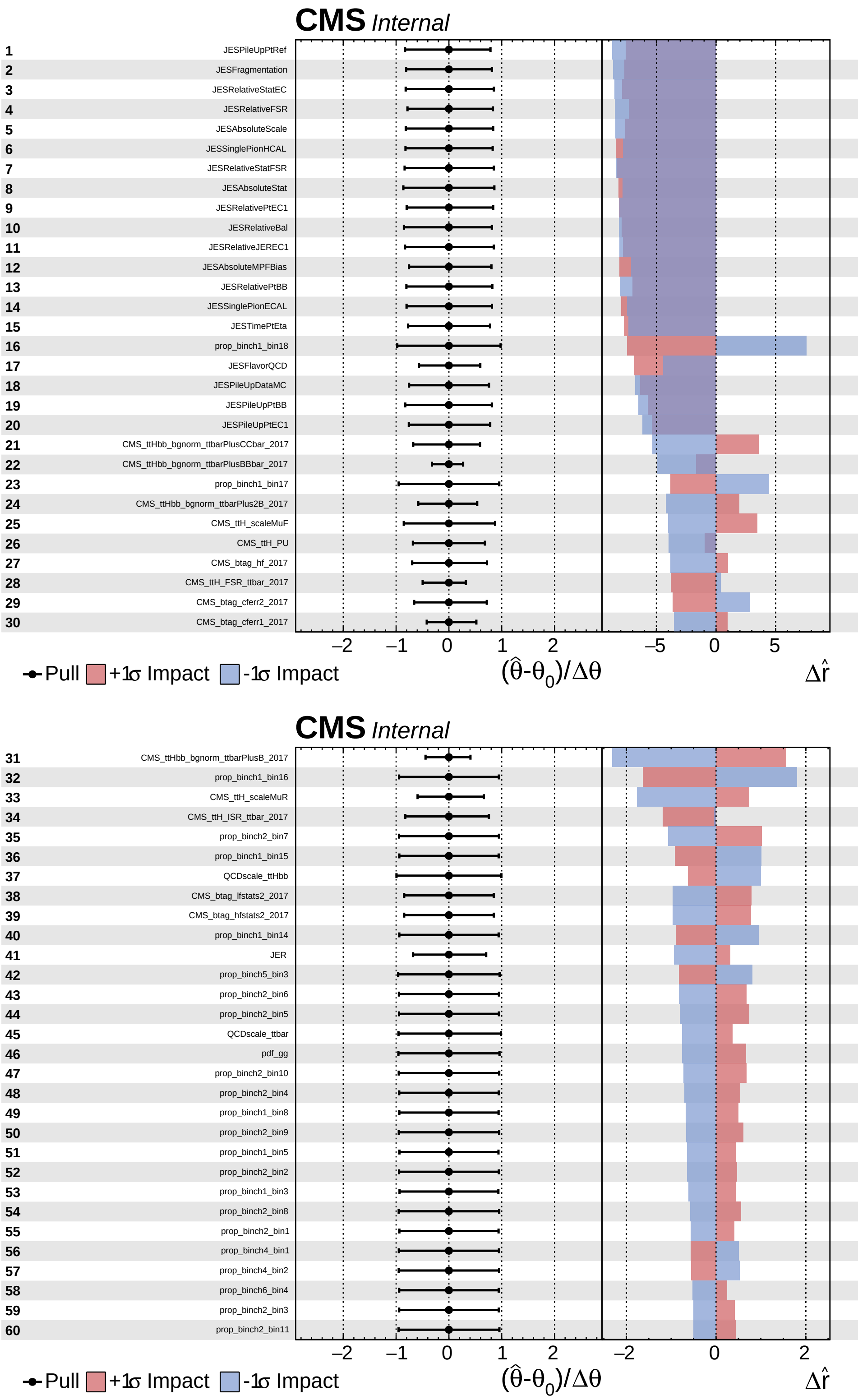

Figure 18. Nuisance parameter pulls and impacts, sorted by the largest impact, obtained from a fit to Asimov data corresponding to the 2017 dataset for the 110 nuisance parameters ranked highest in impact. Continued in Figure 19.

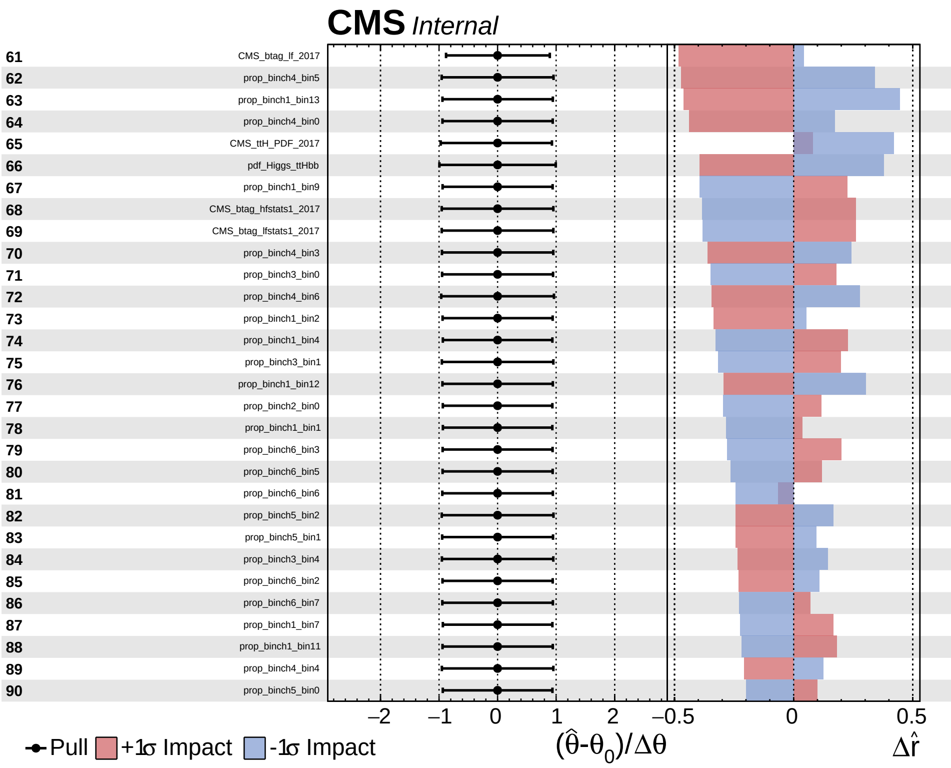

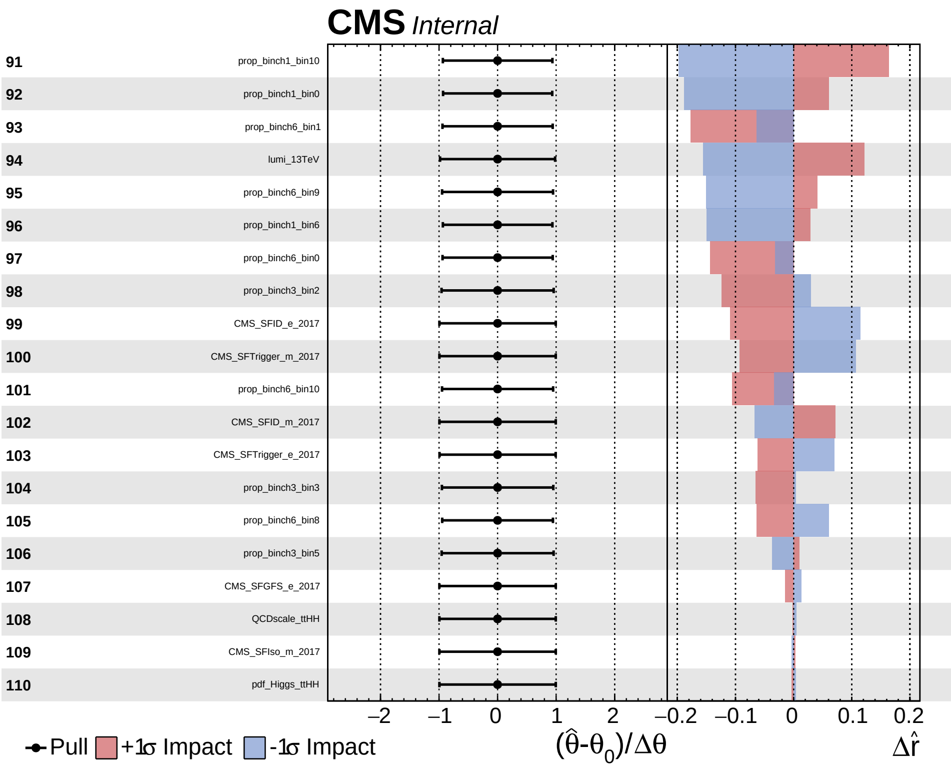

Figure 19. Continued from Figure 18

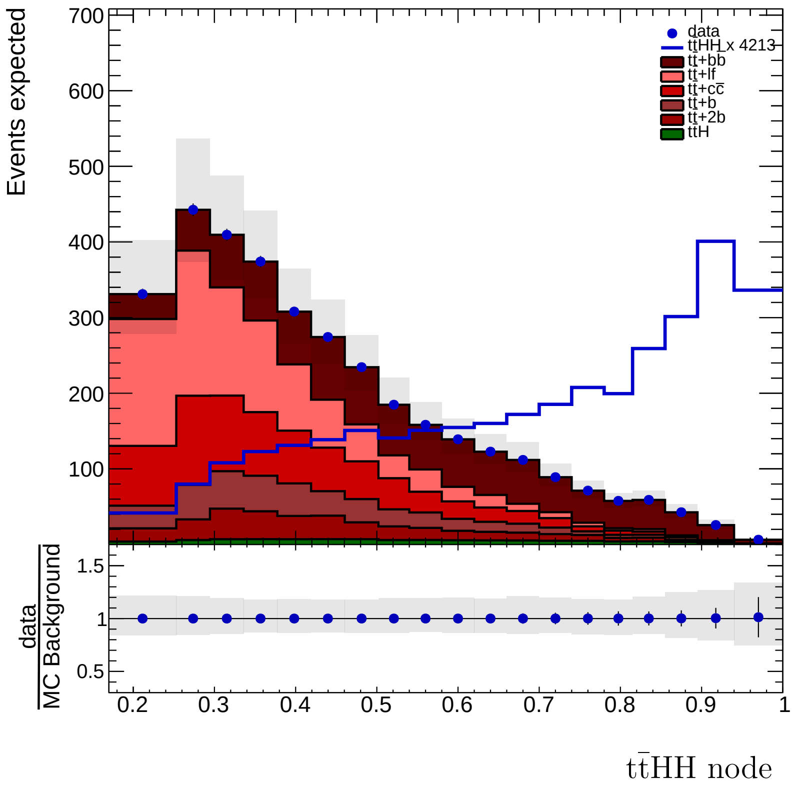

Figure 20. Final discriminant distribution for the signal node, constructed with signal and background processes listed in Table 11 and normalized to 41.5 fb^{-1} luminosity. Data presented here is Asimov data.

7.3.4 Case 4

This case considers at least 6 expected background events in each bin of the signal node, in between Cases 1 and 2, thus the exact same binning of Case 3. Figure 20 shows this choice of binning. The shape systematics are also included in these plots and added in quadrature. Data points is Asimov data. JES systematics are not split into the different sources. In this case there is only one inclusive JES systematic but the varied templates are obtained in the same way as in the previous cases. In this case, even if there is a different set of systematic uncertainties plotted in the discriminant distributions for the background nodes, no difference in the plots of Figure 10 is observed and we keep this same figure to represent all cases.

A fit is the performed and results are obtained for the signal strength μ and summarized in Table 20 in the same way done for Cases 1, 2, 3. Impacts and pulls are shown in Figures 21 and 22. These figures show the systematics ranked by impacts and JES becomes a little more constraining now by looking at the pulls, but it is not the most constraining uncertainty. In terms of impacts it goes from 1^{st} to 27^{th} highest impact on the list and the one sided effect on $\Delta\mu$ disappears. More on this will be discussed in Section 8.

No systematics	Best fit (μ)	Observed (Asimov)	$1^{+25.6}_{-22.4}$
	95% CL upper limits on μ	Expected (Median)	53.3
		Expected (68% CL range)	[37.1,76.6]
		Expected (95% CL range)	[27.5,106.3]
All systematics (excluding bin-by-bin statistics)	Best fit (μ)	Observed (Asimov)	$1^{+29.8}_{-25.7}$
	95% CL upper limits on μ	Expected (Median)	63.0
		Expected (68% CL range)	[43.6,92.9]
		Expected (95% CL range)	[32.0,132.2]
All systematics	Best fit (μ)	Observed (Asimov)	$1^{+31.1}_{-27.5}$
	95% CL upper limits on μ	Expected (Median)	65.5
		Expected (68% CL range)	[45.4,96.1]
		Expected (95% CL range)	[33.3,136.7]

Table 20. Asimov Results. Same as Case 3 with inclusive JES systematic.

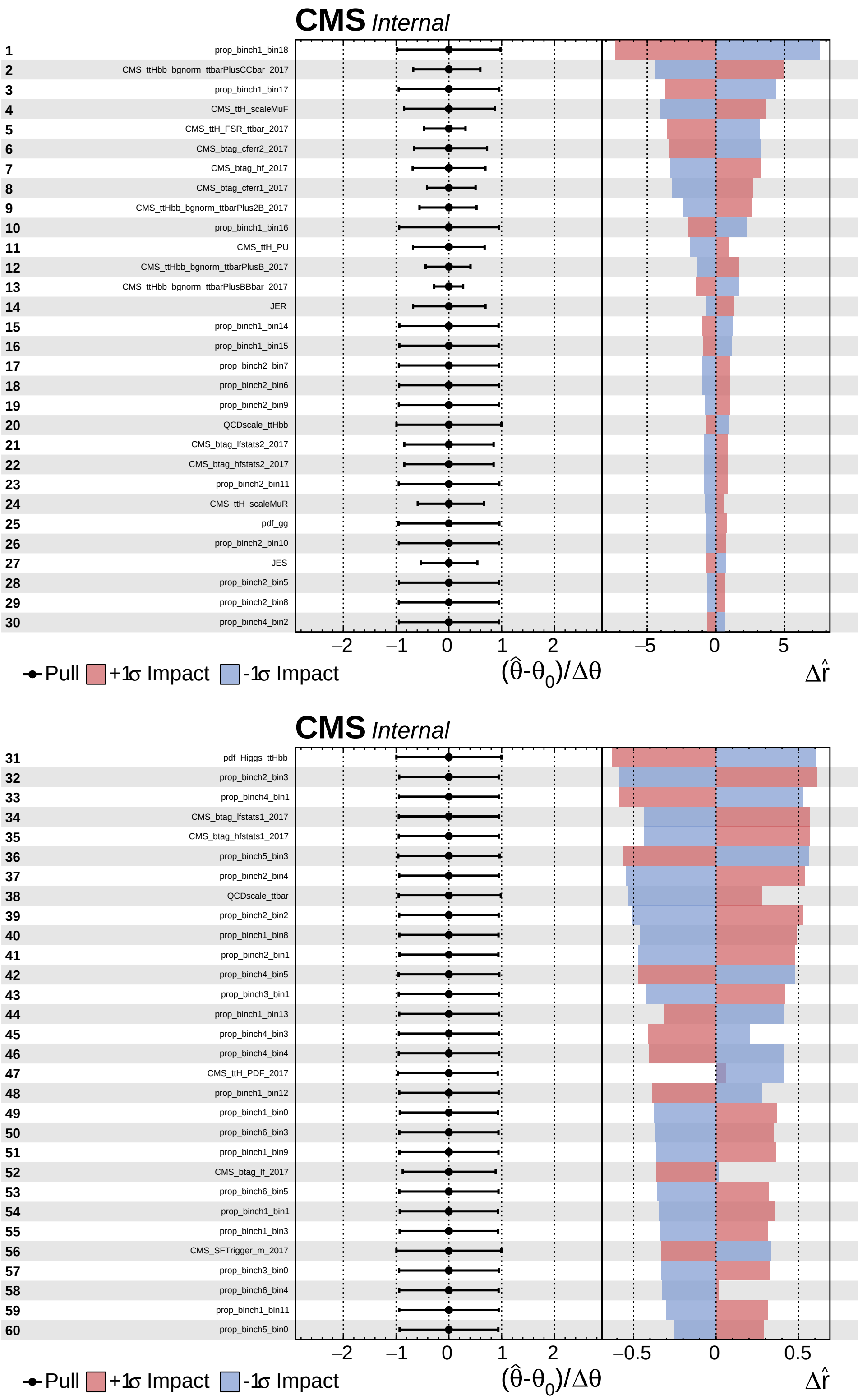

Figure 21. Nuisance parameter pulls and impacts, sorted by the largest impact, obtained from a fit to Asimov data corresponding to the 2017 dataset for the 110 nuisance parameters ranked highest in impact. Continued in Figure 22.

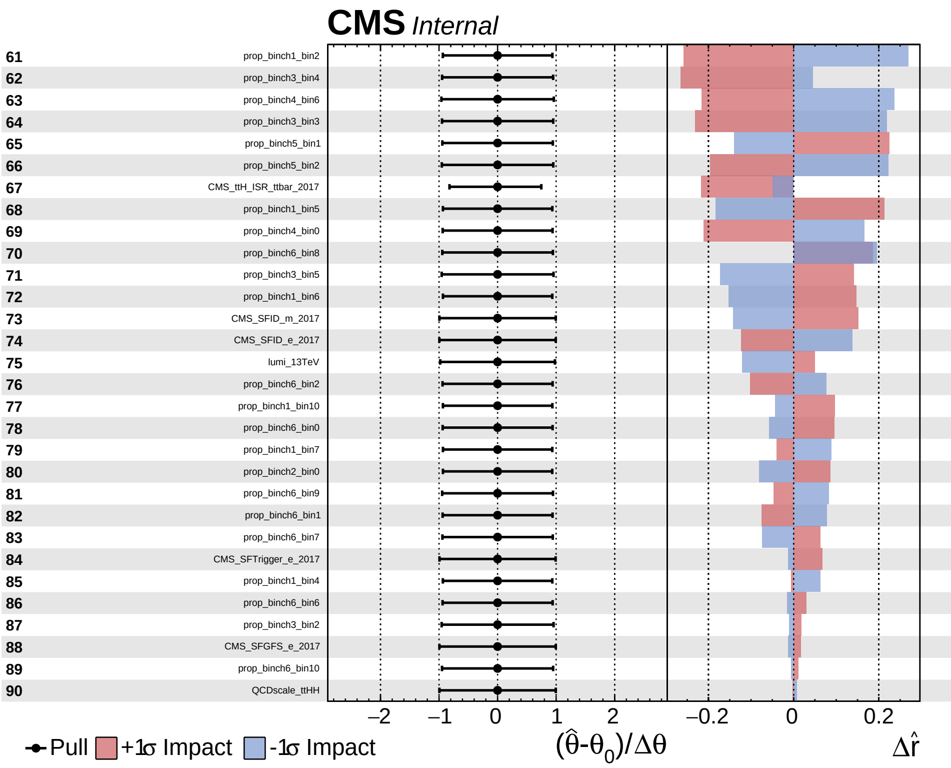

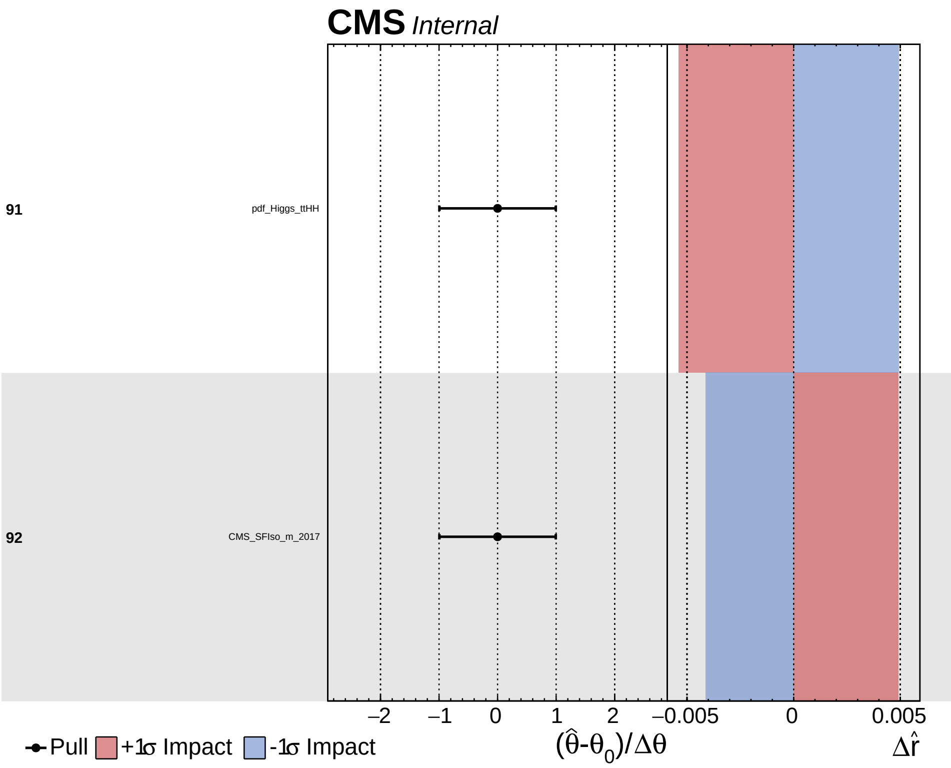

Figure 22. Continued from Figure 21

8 Results and perspectives

Case 4 from Section 7 is chosen as the final result. It keeps 6 events in the last signal bin, as in Case 3, but the scale uncertainty is included in an inclusive JES systematic. It does not consider the individual sources as in Cases 1 to 3. This looks reasonable for this analysis as it is dominated by statistical uncertainties and the inclusive JES systematic, although more constraining than when considering the individual sources, is not too constraining (see Figure 21). This avoids the one sided JES uncertainties of Cases 1 to 3. The JES uncertainty, when considered as individual sources, show a very small, and in some cases no difference, in the plots of nominal shapes when compared to up/sown variations.

The analysis, is dominated by statistics. However, the most constraining systematics are: b tag charm (linear), PS scale: FSR($t\bar{t}$), addition al 50 % rate uncertainty on $t\bar{t}+b\bar{b}$ and $t\bar{t}+b$ cross section, which be seen in the nuisance parameter plots of Figure 21 and 22.

Table 21 summarizes the final result obtained for this analysis. It is worth mentioning that these results are not too different from the results obtained on cases 1 to 3.

Best fit (μ)	Observed (Asimov)	$1^{+31.1}_{-27.5}$
95% CL upper limits on μ	Expected (Median)	65.5
	Expected (68% CL range)	[45.4,96.1]
	Expected (95% CL range)	[33.3,136.7]

Table 21. Final result after fitting to Asimov data including all systematic uncertainties. This is Case 4 of Section 7.

8.1 Perspectives

In this section, the following Tables summarizes a first estimate on the μ-parameter 2017-Run results. This takes into account only the $t\bar{t}$ (SL)HH(4b's) signature for the overall Run 2 (Lumi×3) and for Run 3 (Lumi×10). Run 3 is computed at 13 TeV center of mass energy instead of 14 TeV in this first estimate. This first estimate will be further developed in the upcoming full Run 2 and Run 3 analysis. A number of improvements besides the increase in luminosity will be included in these new analyses, for instance the new b-tagging, the improved $t\bar{t}$-background, especially $t\bar{t}+4b$ and hopefully larger statistics on $t\bar{t}$ overall background, including $t\bar{t}H$ and also the splitting of the JES systematic into the different sources.

Tables 22, 23, 24 and 25 represent the Cases 1, 2, 3, 4 of Section 7.3 respectively. There is not so much different in the results of the different cases.

8.2 Overall Plan for the $t\bar{t}$HH search: from now to High Luminosity LHC

At the dawn of Run 3 and HL-LHC it is important to stress the interest of the $t\bar{t}$HH analysis and to carry on the current exploratory study i.e. $t\bar{t}$ (SL)HH(4b) first on the

Luminosity	Best-fit μ	95% CL limits on μ		
		Expected		
		Median	68% CL Range	95% CL Range
41.5	$1^{+26.4}_{-20.2}$	58.3	[39.4,87.5]	[28.2,126.7]
41.5∗3	$1^{+14.8}_{-13.5}$	31.6	[21.7,46.9]	[15.8,67.1]
41.5∗10	$1^{+9.1}_{-8.2}$	16.8	[11.7,24.5]	[8.7,34.6]

Table 22. Luminosity Scaling for Case 1.

Luminosity	Best-fit μ	95% CL limits on μ		
		Expected		
		Median	68% CL Range	95% CL Range
41.5	$1^{+31.3}_{-29.7}$	65.5	[45.5,95.5]	[33.5,135.6]
41.5∗3	$1^{+18.4}_{-18.9}$	37.6	[26.6,54.1]	[19.7,75.3]
41.5∗10	$1^{+10.5}_{-11.4}$	21.2	[15.1,30.1]	[11.3,41.3]

Table 23. Luminosity Scaling for Case 2

Luminosity	Best-fit μ	95% CL limits on μ		
		Expected		
		Median	68% CL Range	95% CL Range
41.5	$1^{+29.8}_{-27.5}$	63.0	[43.6,92.9]	[32.0,132.2]
41.5∗3	$1^{+17.4}_{-17.6}$	35.9	[25.2,52.0]	[18.6,72.8]
41.5∗10	$1^{+10.0}_{-10.7}$	20.2	[14.3,28.8]	[10.7,39.6]

Table 24. Luminosity Scaling for Case 3

Luminosity	Best-fit μ	95% CL limits on μ		
		Expected		
		Median	68% CL Range	95% CL Range
41.5	$1^{+29.8}_{-25.7}$	63.0	[43.6,92.9]	[32.0,132.2]
41.5∗3	$1^{+19.6}_{-18.6}$	40.3	[28.4,58.1]	[21.1,80.9]
41.5∗10	$1^{+13.7}_{-13.2}$	27.8	[19.8,39.6]	[14.7,54.5]

Table 25. Luminosity scaling for Case 4

overall Run 2 and also to include the other top pair decay channels with Run 2 data and pursue with Run 3 and HL-LHC Here below the preliminary workplan and expected main outcomes is presented:

– With O(40) total events in the 2017 Run period, the signature under study is $t\bar{t}$ (SL)HH(4b) where it is expected O(5 events). Results are being documented in this present analysis Note. It is the first time this data analysis is achieved.

– With O(140) total events for all All Run 2, the signature $t\bar{t}$ (SL)HH(4b) has O(18 events) expected. In this case the 2017 analysis will be redone with Run 2; It starts now with Run 2 $t\bar{t}H(b\bar{b})$ frame including New DNN cat. with $t\bar{t}H$ bkgd and $t\bar{t}+4b$; Fit eval. considering the effect of ttZ and ttZZ and results by Summer 2020. All $t\bar{t}$ signatures (O(50 events)) is expected to start by March 2020 and results ready by Spring 2021 (at least with all hadronic case).

– With O(400) (14TeV) total events for Run 3, all signatures are to be considered with $t\bar{t}+4b$ @NLO background. Here it is expected a first evidence for the $t\bar{t}HH$ process and a possible observation of a deviation from SM.

– With O(4000) total events (14 TeV) for HL LHC, all signatures are expected to be studied with $t\bar{t}+4b$ @NLO and new $t\bar{t}H$, ttZ, ttZZ backgrounds included. Here an evidence of the $t\bar{t}HH$ process is expected as well as a deviation from SM. If increased, it will reject some MCHM scenarios. The study will be combined with heavy resonance search. The triple H search with complementary inputs to double Higgs will be addressed..

9 Concluding Remarks

Acknowledgments

This work was supported by the São Paulo Research Foundation (FAPESP) under Grants No. 2016/01343-7, No. 2013/01907-0, No. 2015/26624-6 and No. 2018/11505-0 and by Science Without Borders/CAPES for UNESP-SPRACE under the Grant No. 88887.116917/2016-00.

A DNN Input Variables

Table 26. Input variables used in the DNNs (Continued in Table 27.)

Variable	Definition
BLR	likelihood ratio discriminating between events with 4 b-quark jets and 2 b-quark jets
$\mathrm{BLR}^{\mathrm{trans}}$	$\ln[\mathrm{BLR}/(1-\mathrm{BLR})]$
p_{T} (jet 1)	p_{T} of the 1^{st} jet, ranked in jet p_{T}
p_{T} (jet 2)	p_{T} of the 2^{nd} jet, ranked in jet p_{T}
p_{T} (jet 3)	p_{T} of the 3^{rd} jet, ranked in jet p_{T}
p_{T} (jet 4)	p_{T} of the 4^{th} jet, ranked in jet p_{T}
H_T^b	scalar sum of p_{T} of b-tagged jets
H_T	scalar sum of p_{T} of all jets
$\mathrm{N}_b^{\mathrm{loose}}$	number of b-tagged jets with DeepCSV > 0.1522
$\mathrm{N}_b^{\mathrm{medium}}$	number of b-tagged jets with DeepCSV > 0.4941
$\mathrm{N}_b^{\mathrm{tight}}$	number of b-tagged jets with DeepCSV > 0.8001
$\mathrm{N}_{\mathrm{jets}}$	number of jets
d(jet 1)	b-tagging discriminant value of 1^{st} jet, ranked in jet p_{T}
d(jet 2)	b-tagging discriminant value of 2^{nd} jet, ranked in jet p_{T}
d(jet 3)	b-tagging discriminant value of 3^{rd} jet, ranked in jet p_{T}
d(jet 4)	b-tagging discriminant value of 4^{th} jet, ranked in jet p_{T}
d_1	1^{st} highest b-tagging discriminant value of all jets
d_2	2^{nd} highest b-tagging discriminant value of all jets
d_3	3^{rd} highest b-tagging discriminant value of all jets
d_4	4^{th} highest b-tagging discriminant value of all jets
$\mathrm{d}_j^{\mathrm{avg}}$	average b-tagging discriminant value of all jets
$\mathrm{d}_b^{\mathrm{avg}}$	average b-tagging discriminant value of all b-tagged jets
$\mathrm{d}_b^{\mathrm{min}}$	minimal b-tagging discriminant value of all b-tagged jets
$\mathrm{d}_j^{\mathrm{min}}$	minimal b-tagging discriminant value of all jets
$\frac{1}{N_b}\Sigma_b^{N_b}(d-d_b^{\mathrm{avg}})^2$	squared difference between the b-tagged discriminant value of a b-tagged jet and the average b-tagging discriminant value of all b-tagged jets, averaged over all b-tagged jets
$\frac{1}{N_j}\Sigma_j^{N_j}(d-d_j^{\mathrm{avg}})^2$	squared difference between the b-tagged discriminant value of a jet and the average b-tagging discriminant value of all jets, averaged over all jets

Table 27. Continued from Table 26.

Variable	Definition
m_j^{avg}	average mass of all jets
$m_{b,b}^{\text{closest to 125}}$	mass of pair of b-tagged jets closest to 125 GeV
$m_{\text{lep},b}^{\min\Delta R}$	mass of pair of lepton and b-tagged jet closest in ΔR
$m_{j,j}^{\min\Delta R}$	mass of pair of jets closest in ΔR
$m_{b,b}^{\min\Delta R}$	mass of pair of b-tagged jets closest in ΔR
$m_{\text{lep},j}^{\min\Delta R}$	mass of pair of lepton and jet closest in ΔR
m_b^{avg}	average mass of all b-tagged jets
$(m^2)_b^{avg}$	average squared mass of all b-tagged jets
$\Delta R_{\text{b,b}}^{\text{avg}}$	average ΔR between b-tagged jets
$\Delta R_{\text{j,j}}^{\text{avg}}$	average ΔR between two jets
$\Delta R_{\text{j,j}}^{\text{min}}$	minimal ΔR between any two jets
$\Delta R_{\text{b,b}}^{\text{min}}$	minimal ΔR between any two b-tagged jets
$\Delta R_{\text{lep,b}}^{\text{min}}$	minimal ΔR between lepton and b-tagged jet
$\Delta R_{\text{lep,j}}^{\text{min}}$	minimal ΔR between lepton and jet
$\Delta\eta_{\text{j,j}}^{\text{avg}}$	average $\Delta\eta$ between any two jets
$\Delta\eta_{\text{b,b}}^{\text{avg}}$	average $\Delta\eta$ between any two b-tagged jets
$\Delta\eta_{\text{b,b}}^{\text{max}}$	largest $\Delta\eta$ between any two b-tagged jets
${p_{\text{T}}}_{\text{j}}^{\text{avg}}/\text{E}_{\text{j}}^{\text{avg}}$	average jet p_{T} over average jet E of all jets
H_0	0th Fox–Wolfram moment [29] computed with all jets
H_1	1st Fox–Wolfram moment [29] computed with all jets

A.1 Input Variable Control Plots

Data/MC comparisons of the observables used as inputs to DNN used to produce the final discriminants before the fit to data. Each of the expected backgrounds is normalized to the corresponding SM cross section.

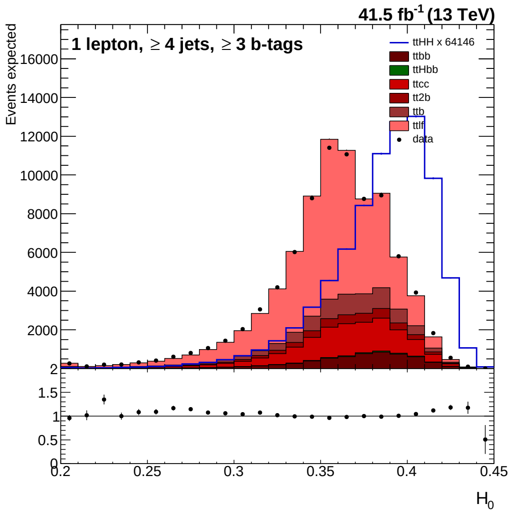

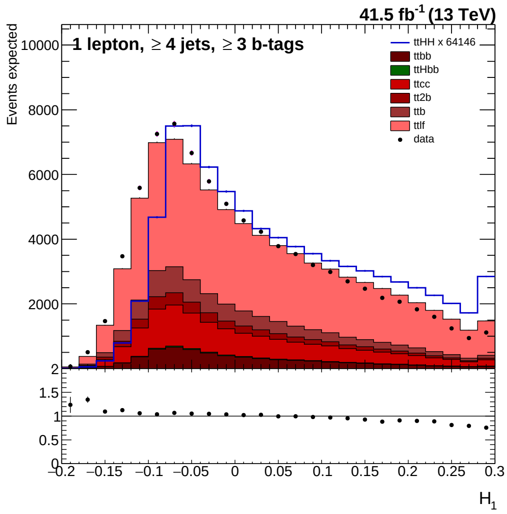

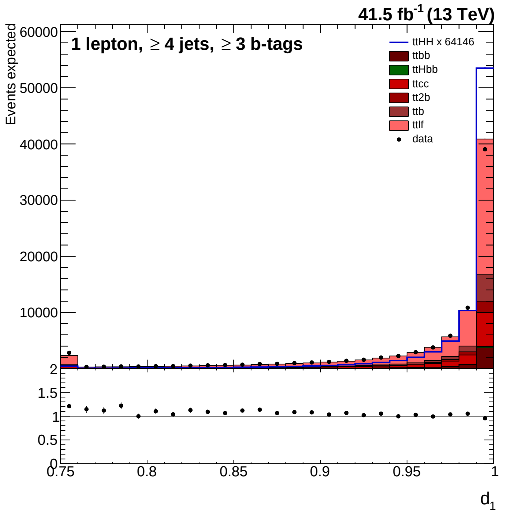

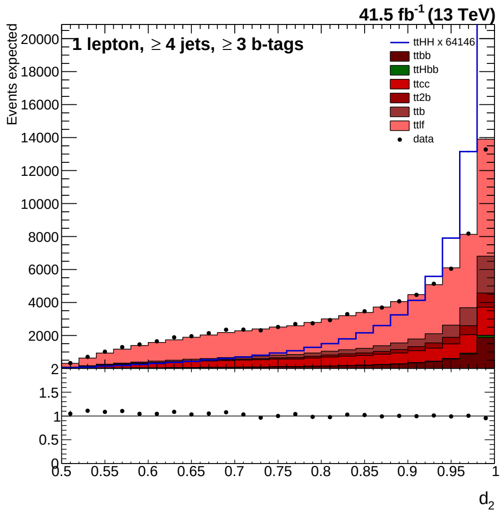

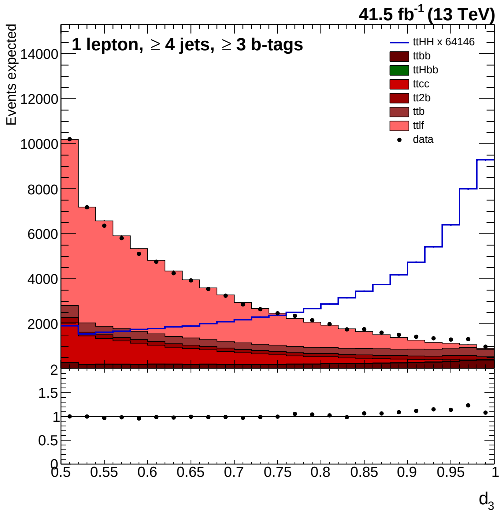
41.5 fb^{-1} (13 TeV)
1 lepton, ≥ 4 jets, ≥ 3 b-tags
ttHH x 64146
ttbb
ttHbb
ttcc
tt2b
ttb
ttlf
data
Events expected
d_3

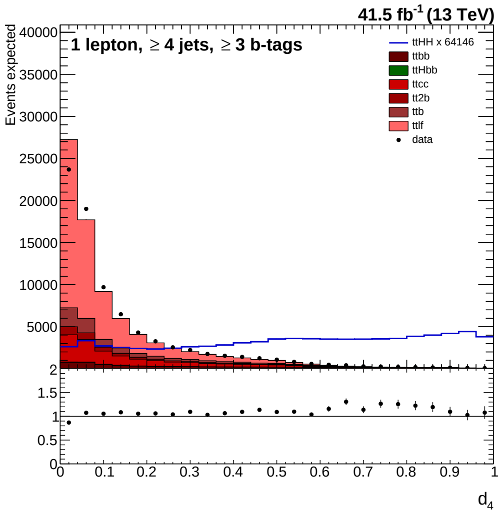
41.5 fb^{-1} (13 TeV)
1 lepton, ≥ 4 jets, ≥ 3 b-tags
ttHH x 64146
ttbb
ttHbb
ttcc
tt2b
ttb
ttlf
data
Events expected
d_4

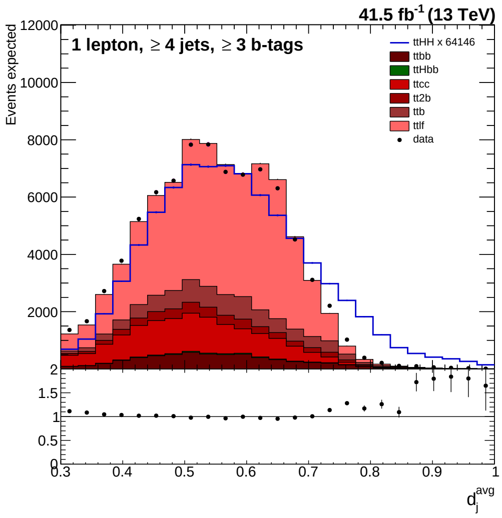
41.5 fb^{-1} (13 TeV)
1 lepton, ≥ 4 jets, ≥ 3 b-tags
ttHH x 64146
ttbb
ttHbb
ttcc
tt2b
ttb
ttlf
data
Events expected
d_j^{avg}

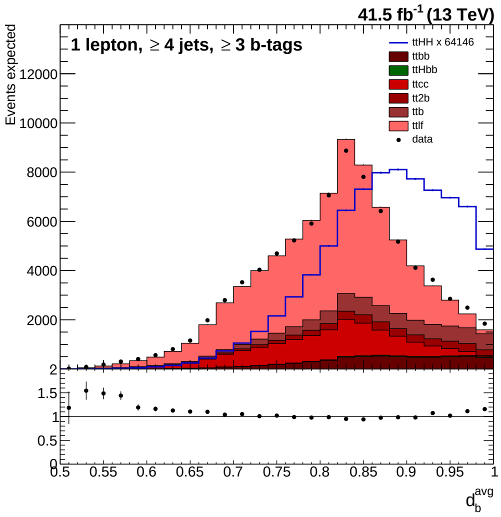
41.5 fb^{-1} (13 TeV)
1 lepton, ≥ 4 jets, ≥ 3 b-tags
ttHH x 64146
ttbb
ttHbb
ttcc
tt2b
ttb
ttlf
data
Events expected
d_b^{avg}

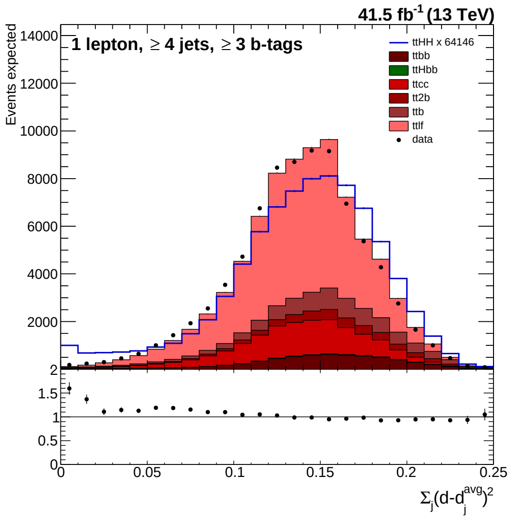
41.5 fb^{-1} (13 TeV)
1 lepton, ≥ 4 jets, ≥ 3 b-tags
ttHH x 64146
ttbb
ttHbb
ttcc
tt2b
ttb
ttlf
data
Events expected
$\Sigma_j(d-d_j^{avg})^2$

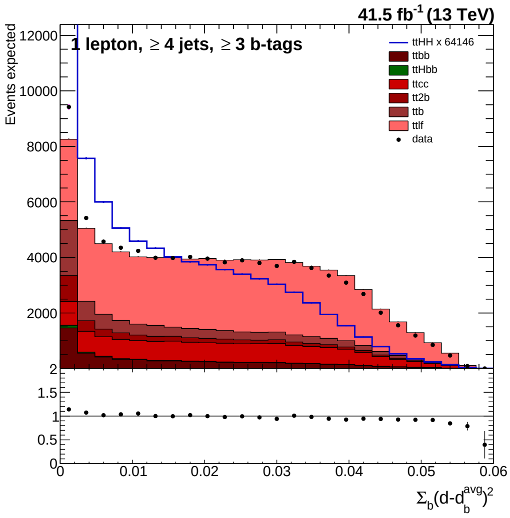
41.5 fb^{-1} (13 TeV)
1 lepton, ≥ 4 jets, ≥ 3 b-tags
ttHH x 64146
ttbb
ttHbb
ttcc
tt2b
ttb
ttlf
data
Events expected
$\Sigma_b(d-d_b^{avg})^2$

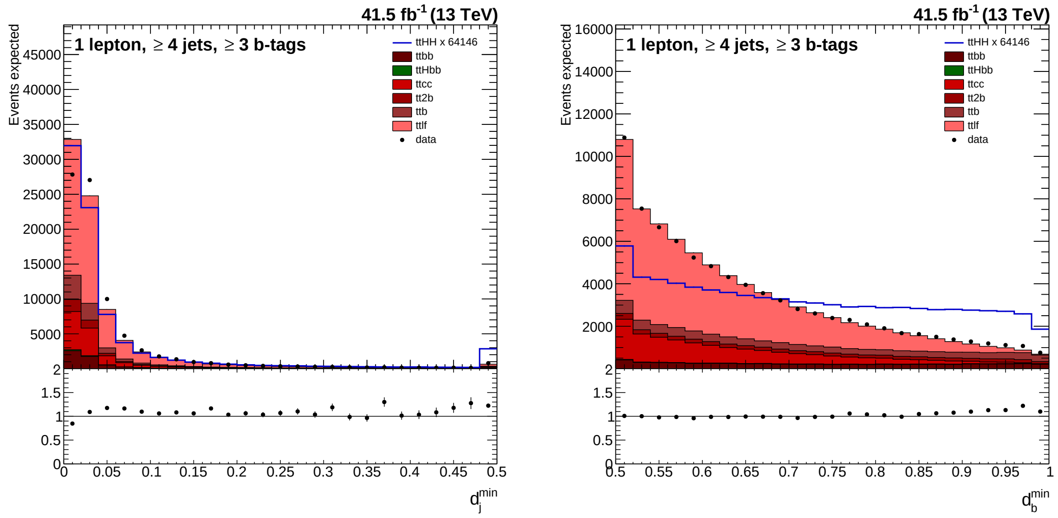
41.5 fb^{-1} (13 TeV)
1 lepton, ≥ 4 jets, ≥ 3 b-tags
ttHH x 64146
ttbb
ttHbb
ttcc
tt2b
ttb
ttlf
data
Events expected
d_j^{min}
d_b^{min}

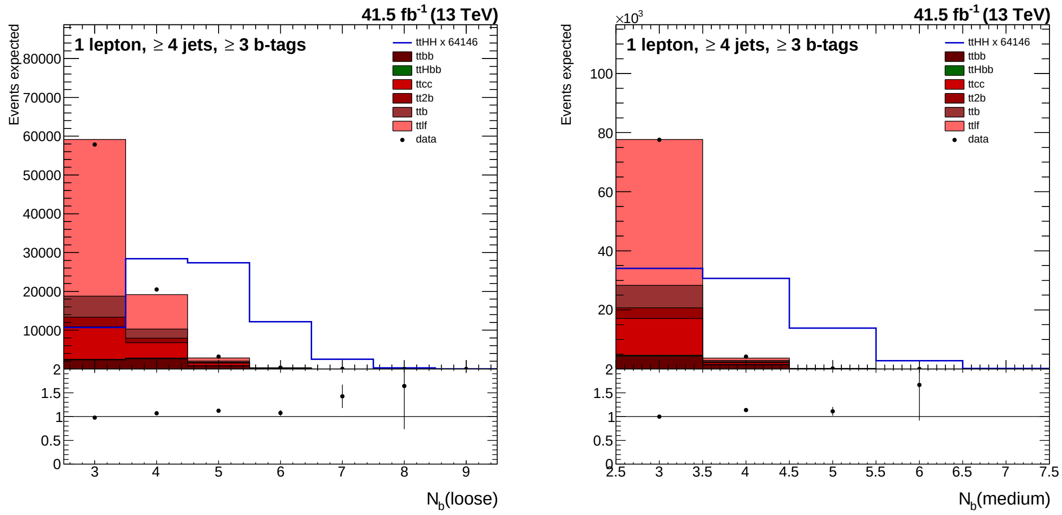
41.5 fb^{-1} (13 TeV)
1 lepton, ≥ 4 jets, ≥ 3 b-tags
ttHH x 64146
ttbb
ttHbb
ttcc
tt2b
ttb
ttlf
data
Events expected
$\times10^3$
N_b(loose)
N_b(medium)

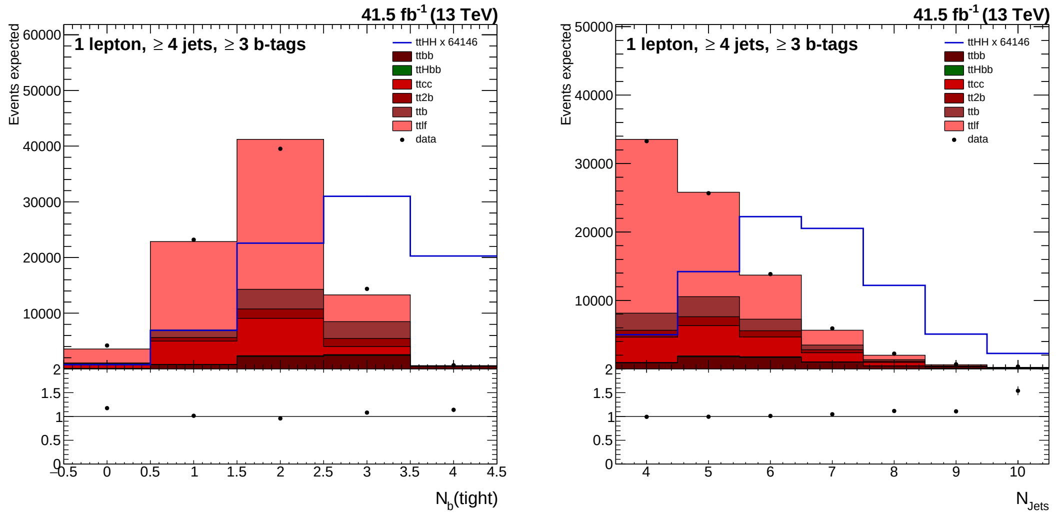
41.5 fb^{-1} (13 TeV)
1 lepton, ≥ 4 jets, ≥ 3 b-tags
ttHH x 64146
ttbb
ttHbb
ttcc
tt2b
ttb
ttlf
data
Events expected
N_b(tight)
N_{Jets}

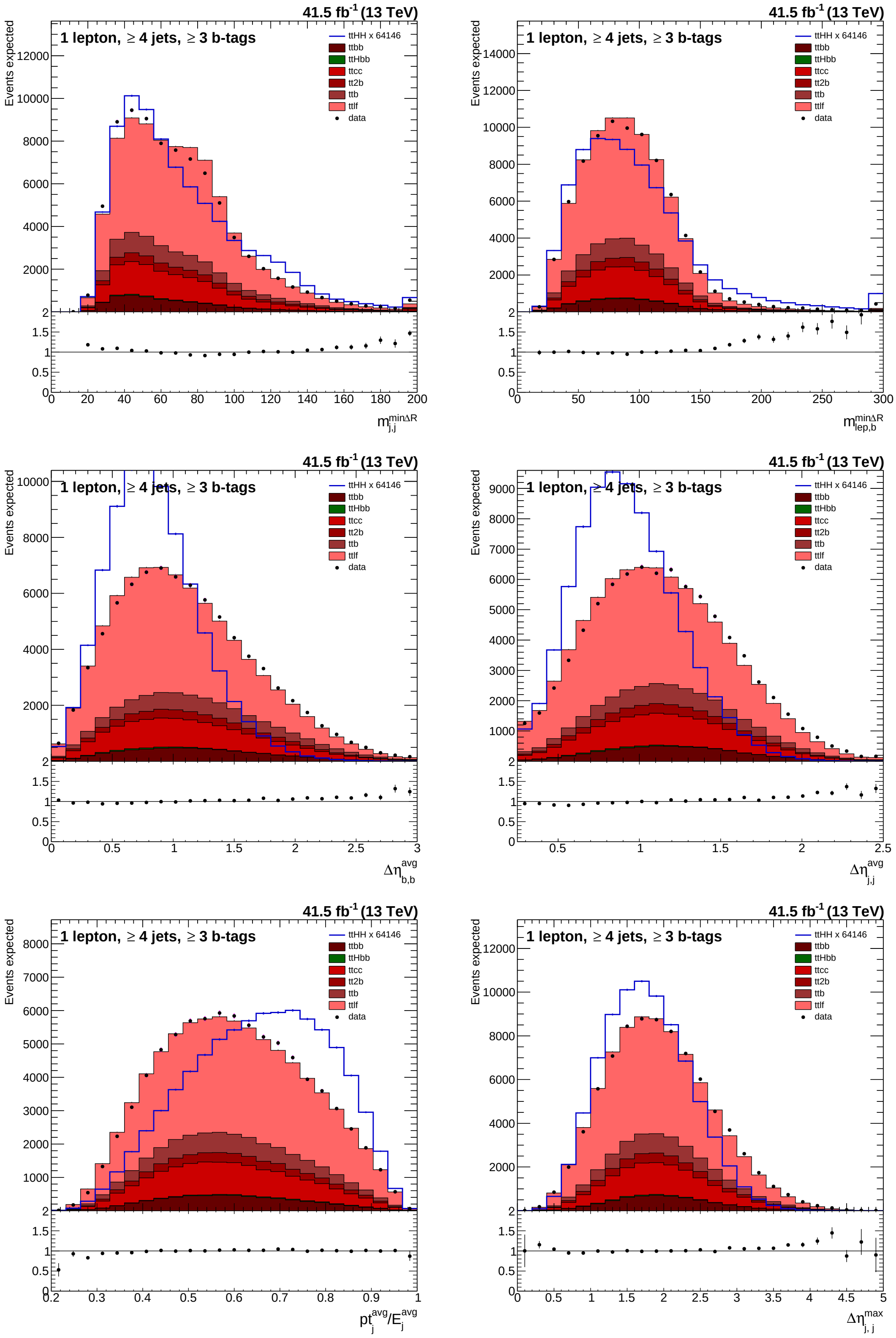
41.5 fb^{-1} (13 TeV)
1 lepton, ≥ 4 jets, ≥ 3 b-tags
Events expected
ttHH x 64146
ttbb
ttHbb
ttcc
tt2b
ttb
ttlf
data
$m_{j,j}^{min\Delta R}$
$m_{lep,b}^{min\Delta R}$
$\Delta\eta_{b,b}^{avg}$
$\Delta\eta_{j,j}^{avg}$
pt_j^{avg}/E_j^{avg}
$\Delta\eta_{j,j}^{max}$

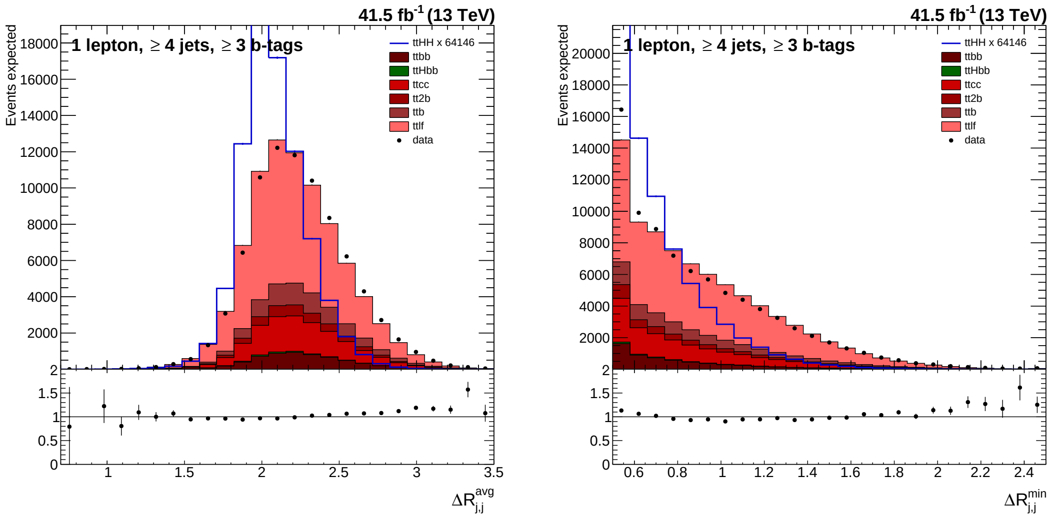
41.5 fb^{-1} (13 TeV)
1 lepton, ≥ 4 jets, ≥ 3 b-tags
ttHH x 64146
ttbb
ttHbb
ttcc
tt2b
ttb
ttlf
data
Events expected
$\Delta R^{avg}_{j,j}$
$\Delta R^{min}_{j,j}$

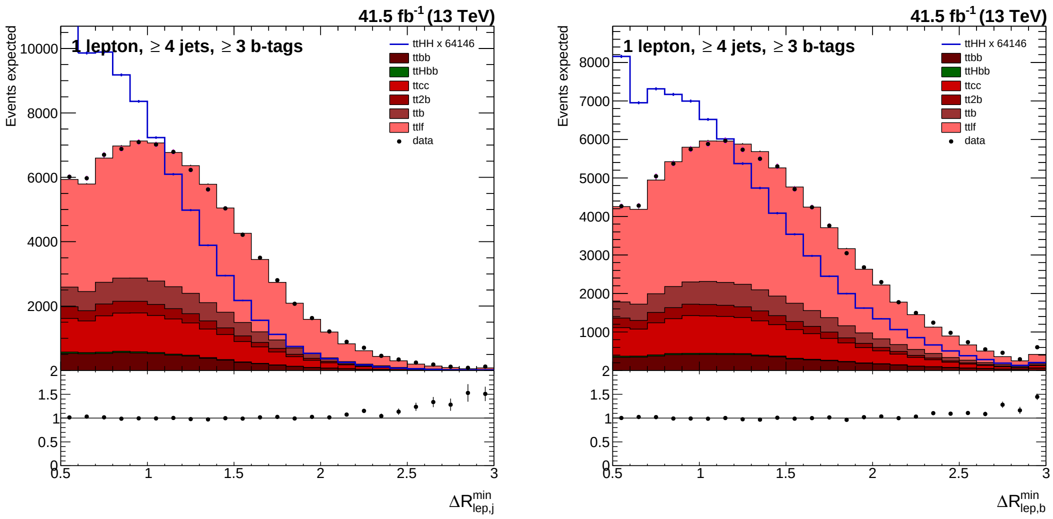
41.5 fb^{-1} (13 TeV)
1 lepton, ≥ 4 jets, ≥ 3 b-tags
ttHH x 64146
ttbb
ttHbb
ttcc
tt2b
ttb
ttlf
data
Events expected
$\Delta R^{min}_{lep,j}$
$\Delta R^{min}_{lep,b}$

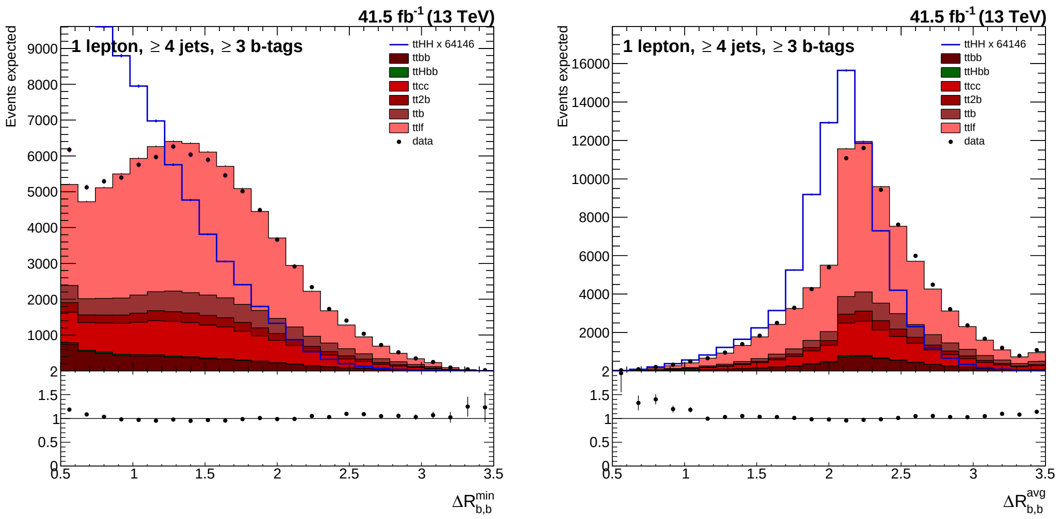
41.5 fb^{-1} (13 TeV)
1 lepton, ≥ 4 jets, ≥ 3 b-tags
ttHH x 64146
ttbb
ttHbb
ttcc
tt2b
ttb
ttlf
data
Events expected
$\Delta R^{min}_{b,b}$
$\Delta R^{avg}_{b,b}$

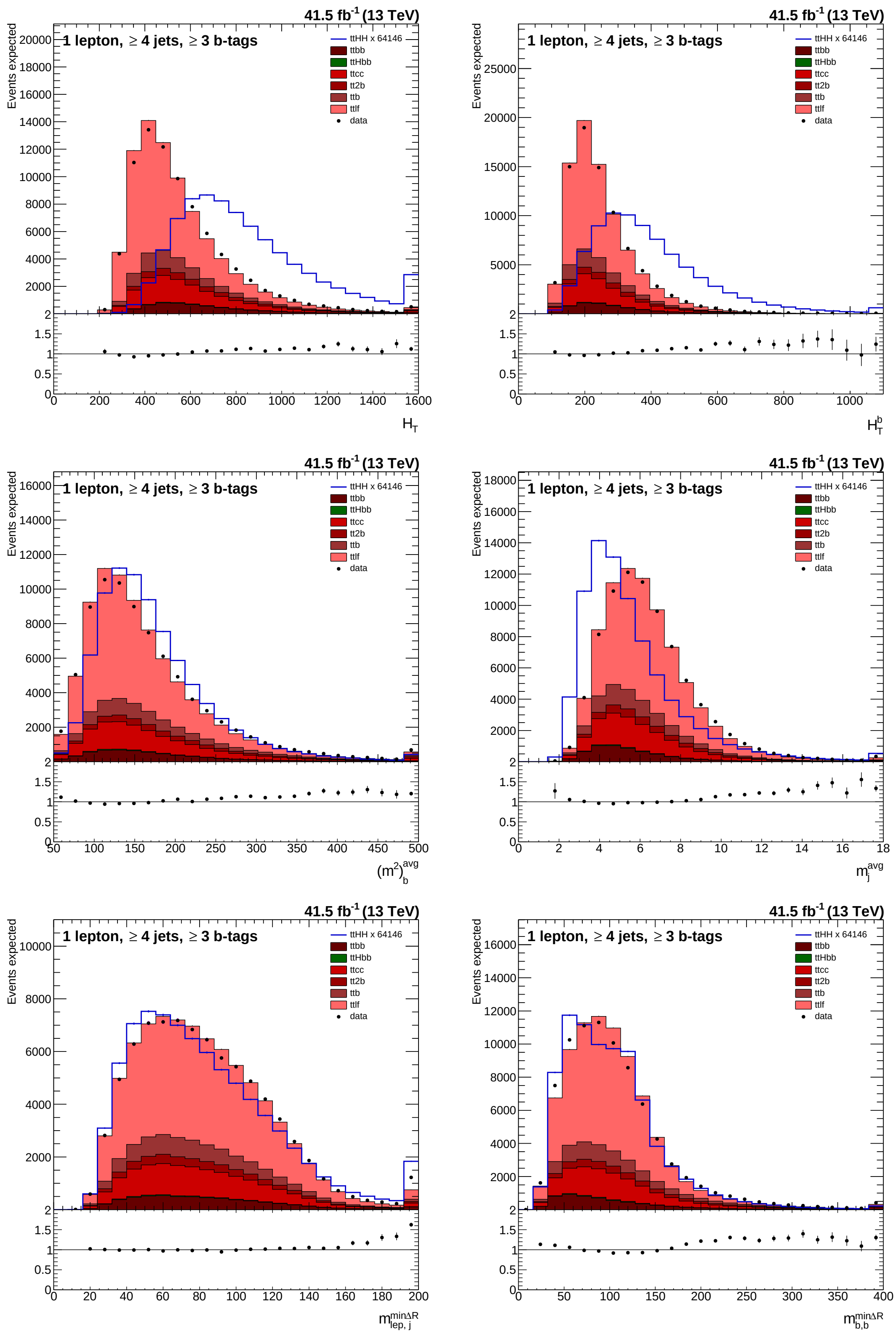
41.5 fb-1 (13 TeV)
1 lepton, ≥ 4 jets, ≥ 3 b-tags
ttHH x 64146
ttbb
ttHbb
ttcc
tt2b
ttb
ttlf
data
Events expected
H_T
H_T^b
(m^2)_b^avg
m_j^avg
m_lep, j^minΔR
m_b,b^minΔR

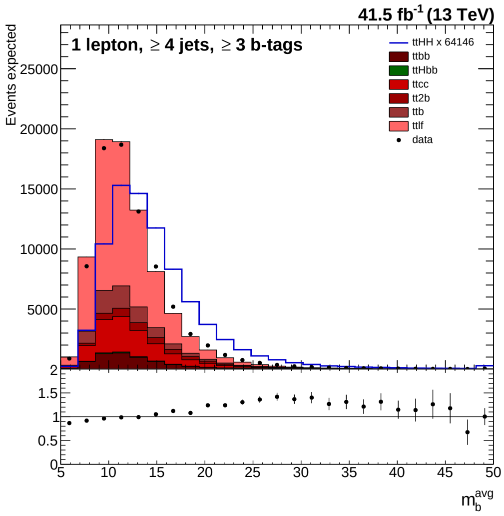
41.5 fb^{-1} (13 TeV)
1 lepton, ≥ 4 jets, ≥ 3 b-tags
ttHH x 64146
ttbb
ttHbb
ttcc
tt2b
ttb
ttlf
data
Events expected
m_b^{avg}

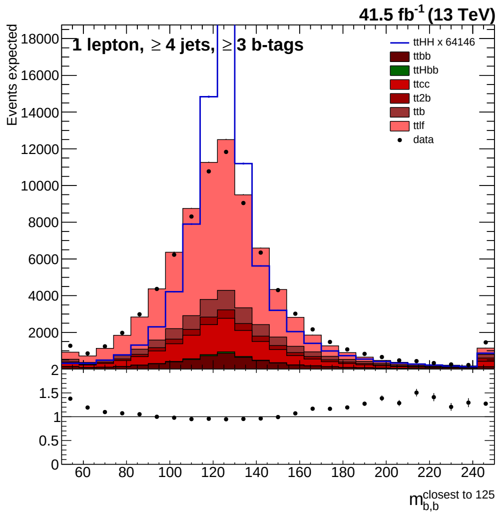
41.5 fb^{-1} (13 TeV)
1 lepton, ≥ 4 jets, ≥ 3 b-tags
ttHH x 64146
ttbb
ttHbb
ttcc
tt2b
ttb
ttlf
data
Events expected
$m_{b,b}^{closest\ to\ 125}$

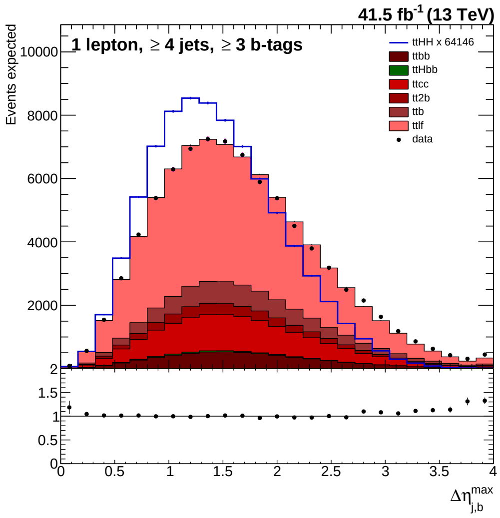
41.5 fb^{-1} (13 TeV)
1 lepton, ≥ 4 jets, ≥ 3 b-tags
ttHH x 64146
ttbb
ttHbb
ttcc
tt2b
ttb
ttlf
data
Events expected
$\Delta\eta_{j,b}^{max}$

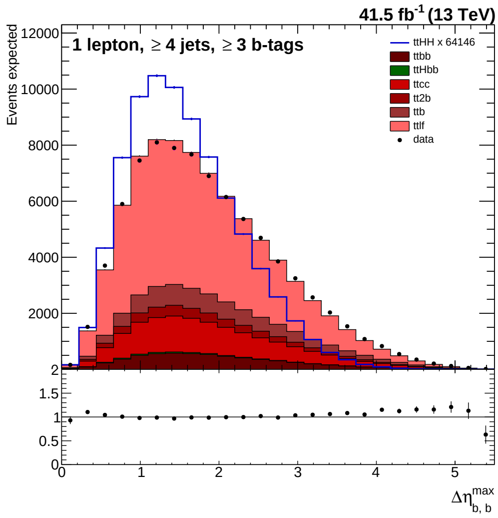
41.5 fb^{-1} (13 TeV)
1 lepton, ≥ 4 jets, ≥ 3 b-tags
ttHH x 64146
ttbb
ttHbb
ttcc
tt2b
ttb
ttlf
data
Events expected
$\Delta\eta_{b,b}^{max}$

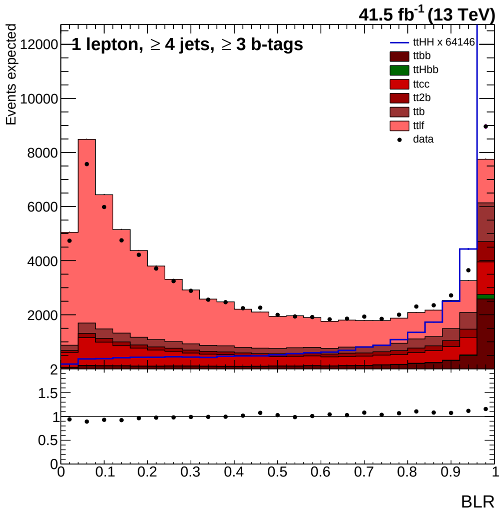
41.5 fb^{-1} (13 TeV)
1 lepton, ≥ 4 jets, ≥ 3 b-tags
ttHH x 64146
ttbb
ttHbb
ttcc
tt2b
ttb
ttlf
data
Events expected
BLR

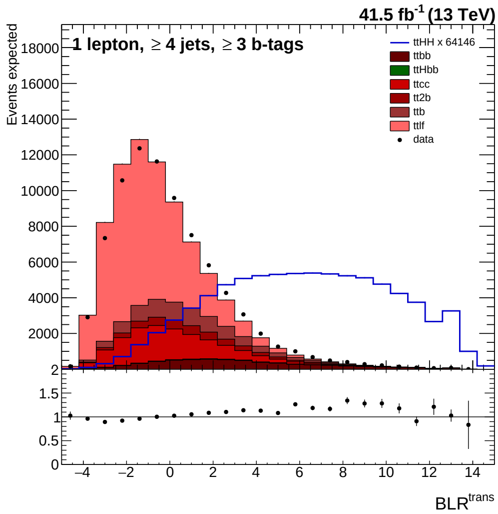
41.5 fb^{-1} (13 TeV)
1 lepton, ≥ 4 jets, ≥ 3 b-tags
ttHH x 64146
ttbb
ttHbb
ttcc
tt2b
ttb
ttlf
data
Events expected
BLR^{trans}

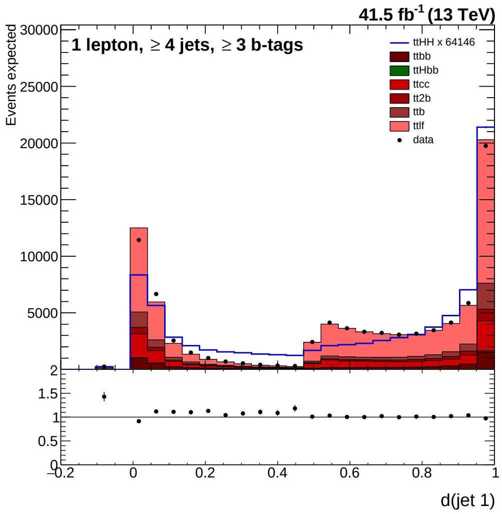
41.5 fb^{-1} (13 TeV)
1 lepton, ≥ 4 jets, ≥ 3 b-tags
ttHH x 64146
ttbb
ttHbb
ttcc
tt2b
ttb
ttlf
data
Events expected
d(jet 1)

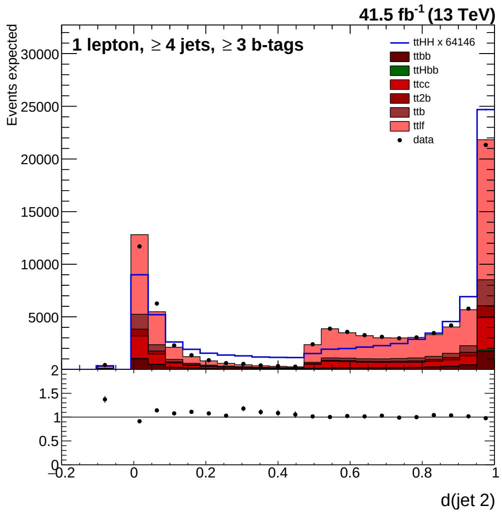
41.5 fb^{-1} (13 TeV)
1 lepton, ≥ 4 jets, ≥ 3 b-tags
ttHH x 64146
ttbb
ttHbb
ttcc
tt2b
ttb
ttlf
data
Events expected
d(jet 2)

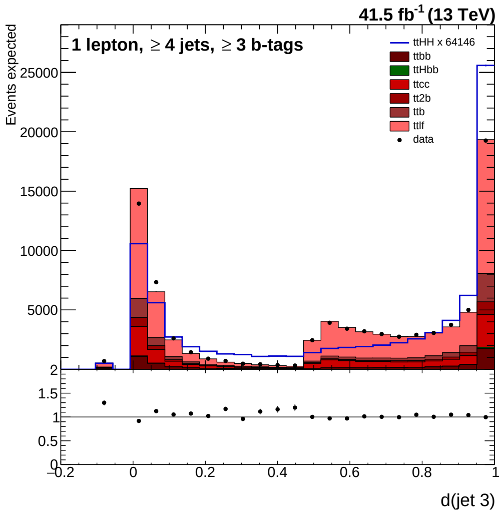
41.5 fb^{-1} (13 TeV)
1 lepton, ≥ 4 jets, ≥ 3 b-tags
ttHH x 64146
ttbb
ttHbb
ttcc
tt2b
ttb
ttlf
data
Events expected
d(jet 3)

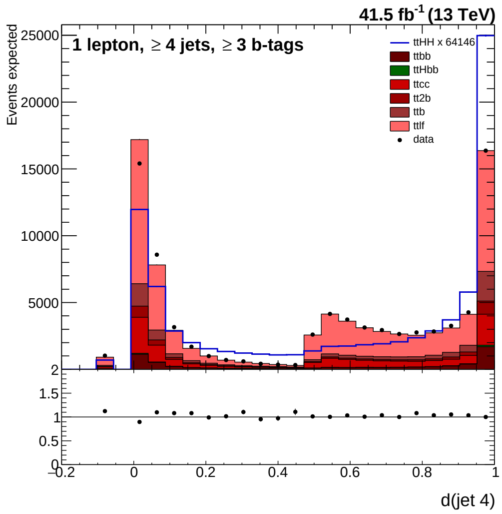
41.5 fb^{-1} (13 TeV)
1 lepton, ≥ 4 jets, ≥ 3 b-tags
ttHH x 64146
ttbb
ttHbb
ttcc
tt2b
ttb
ttlf
data
Events expected
d(jet 4)

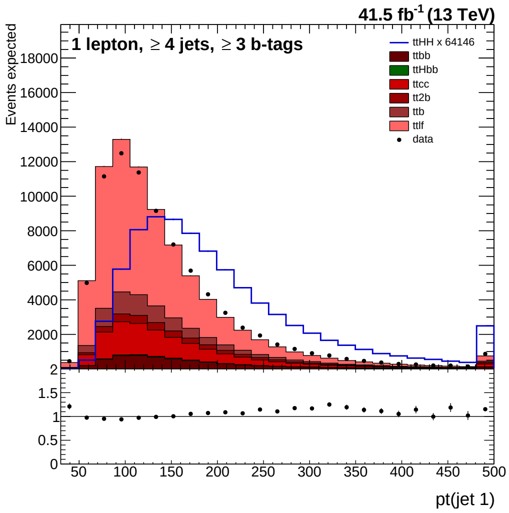
41.5 fb^{-1} (13 TeV)
1 lepton, ≥ 4 jets, ≥ 3 b-tags
ttHH x 64146
ttbb
ttHbb
ttcc
tt2b
ttb
ttlf
data
Events expected
pt(jet 1)

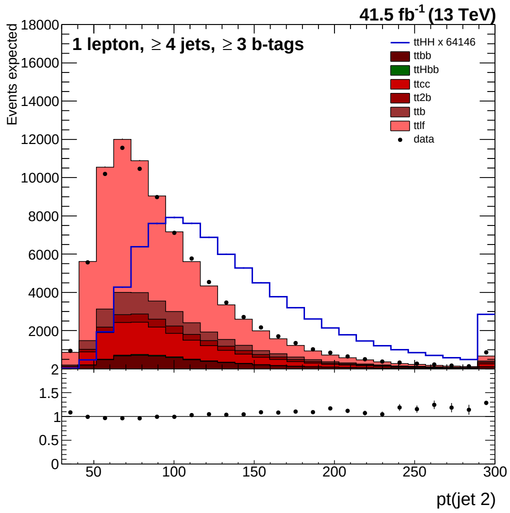
41.5 fb^{-1} (13 TeV)
1 lepton, ≥ 4 jets, ≥ 3 b-tags
ttHH x 64146
ttbb
ttHbb
ttcc
tt2b
ttb
ttlf
data
Events expected
pt(jet 2)

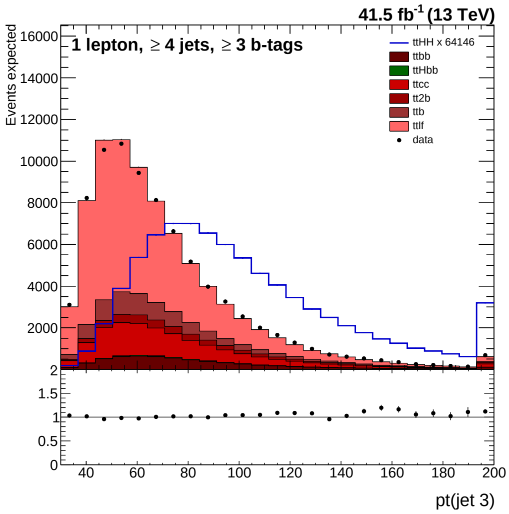
41.5 fb-1 (13 TeV)
1 lepton, ≥ 4 jets, ≥ 3 b-tags
ttHH x 64146
ttbb
ttHbb
ttcc
tt2b
ttb
ttlf
data
Events expected
pt(jet 3)

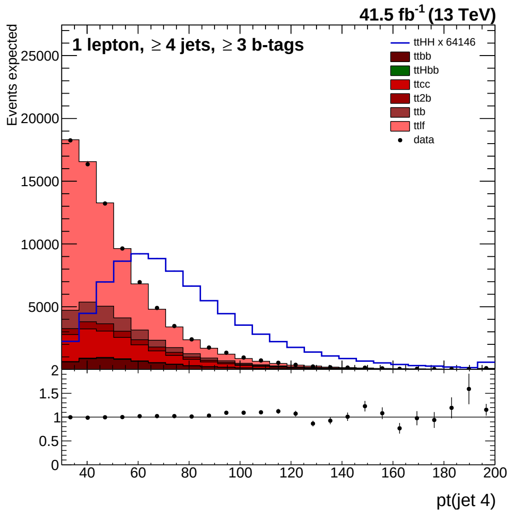
41.5 fb-1 (13 TeV)
1 lepton, ≥ 4 jets, ≥ 3 b-tags
ttHH x 64146
ttbb
ttHbb
ttcc
tt2b
ttb
ttlf
data
Events expected
pt(jet 4)

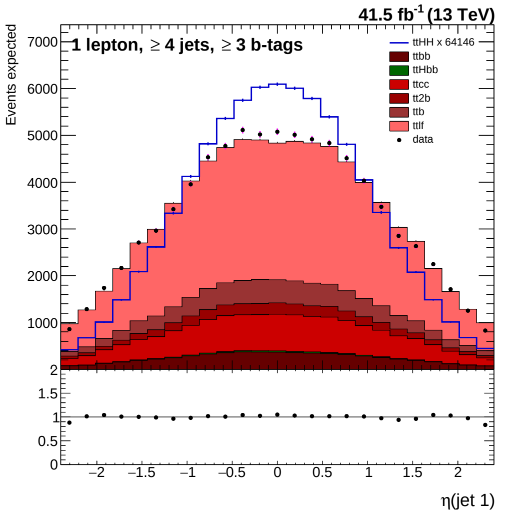
41.5 fb-1 (13 TeV)
1 lepton, ≥ 4 jets, ≥ 3 b-tags
ttHH x 64146
ttbb
ttHbb
ttcc
tt2b
ttb
ttlf
data
Events expected
η(jet 1)

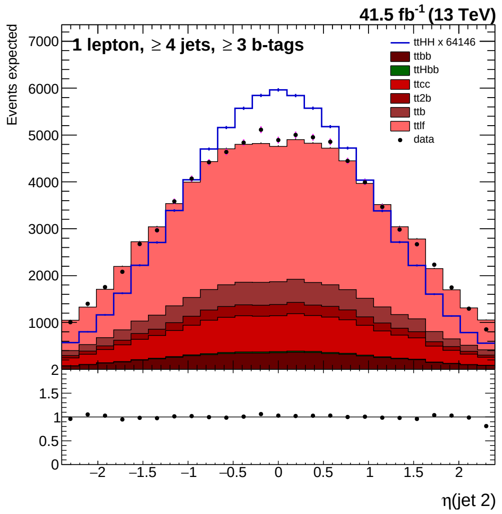
41.5 fb-1 (13 TeV)
1 lepton, ≥ 4 jets, ≥ 3 b-tags
ttHH x 64146
ttbb
ttHbb
ttcc
tt2b
ttb
ttlf
data
Events expected
η(jet 2)

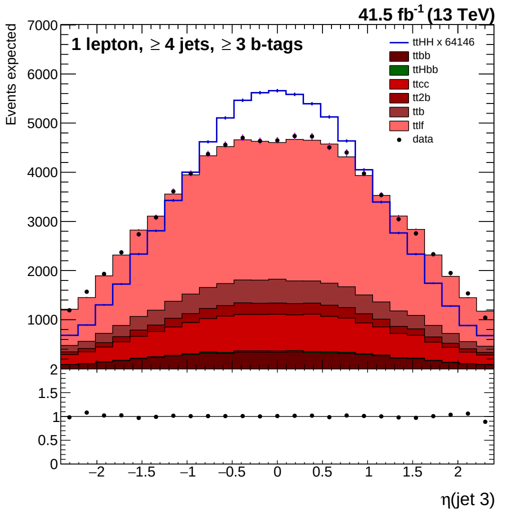
41.5 fb-1 (13 TeV)
1 lepton, ≥ 4 jets, ≥ 3 b-tags
ttHH x 64146
ttbb
ttHbb
ttcc
tt2b
ttb
ttlf
data
Events expected
η(jet 3)

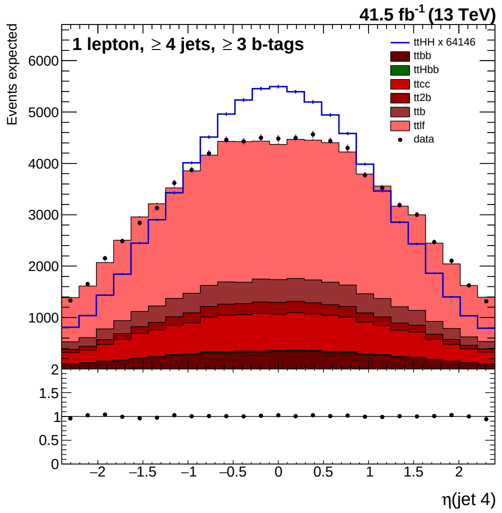
41.5 fb-1 (13 TeV)
1 lepton, ≥ 4 jets, ≥ 3 b-tags
ttHH x 64146
ttbb
ttHbb
ttcc
tt2b
ttb
ttlf
data
Events expected
η(jet 4)

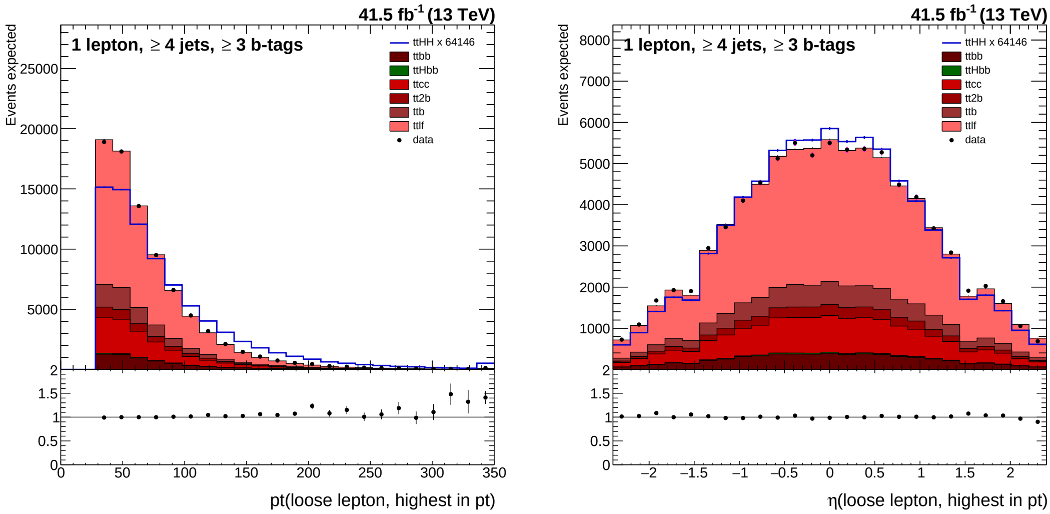
41.5 fb-1 (13 TeV)
1 lepton, ≥ 4 jets, ≥ 3 b-tags
Events expected
ttHH x 64146
ttbb
ttHbb
ttcc
tt2b
ttb
ttlf
data
pt(loose lepton, highest in pt)
41.5 fb-1 (13 TeV)
1 lepton, ≥ 4 jets, ≥ 3 b-tags
Events expected
ttHH x 64146
ttbb
ttHbb
ttcc
tt2b
ttb
ttlf
data
η(loose lepton, highest in pt)

References

[1] CMS collaboration, *Measurement of* $t\bar{t}H$ *production in the* $H \to b\bar{b}$ *decay channel in* $41.5\,fb^{-1}$ *of proton-proton collision data at* $\sqrt{s} = 13\,TeV$, Tech. Rep. CMS-PAS-HIG-18-030, CERN, Geneva, 2019. https://cds.cern.ch/record/2675023.

[2] CMS Collaboration, *Study of the top quark and antiquark pair plus four b-quarks production as a background in the top-higgs sector searches*, CMS Analysis Note 2020/053, CERN, 2020. http://cms.cern.ch/iCMS/jsp/db_notes/noteInfo.jsp?cmsnoteid=CMS%20AN-2020/053.

[3] C. Bautista, L. de Lima, R. Matheus, E. Pontón, L. Fernandes do Prado and A. Savoy-Navarro, *Production of* $t\bar{t}H$ *and* $t\bar{t}HH$ *at the LHC in Composite Higgs models*, to appear.

[4] R. Frederix, S. Frixione, V. Hirschi, F. Maltoni, O. Mattelaer, P. Torrielli et al., *Higgs pair production at the LHC with NLO and parton-shower effects*, *Phys. Lett.* **B732** (2014) 142 [1401.7340].

[5] LHC Higgs Cross Section Working Group collaboration, D. de Florian et al., *Handbook of LHC Higgs Cross Sections: 4. Deciphering the Nature of the Higgs Sector*, 1610.07922.

[6] ATLAS collaboration, G. Aad et al., *Combination of searches for Higgs boson pairs in pp collisions at* $\sqrt{s}$ *=13 TeV with the ATLAS detector*, *Phys. Lett.* **B800** (2020) 135103 [1906.02025].

[7] CMS collaboration, A. M. Sirunyan et al., *Combination of searches for Higgs boson pair production in proton-proton collisions at* $\sqrt{s} =$ *13 TeV*, *Phys. Rev. Lett.* **122** (2019) 121803 [1811.09689].

[8] M. Cepeda et al., *Report from Working Group 2*, *CERN Yellow Rep. Monogr.* **7** (2019) 221 [1902.00134].

[9] ATLAS collaboration, M. Aaboud et al., *Observation of Higgs boson production in association with a top quark pair at the LHC with the ATLAS detector*, *Phys. Lett.* **B784** (2018) 173 [1806.00425].

[10] CMS collaboration, A. M. Sirunyan et al., *Observation of* $t\bar{t}H$ *production*, *Phys. Rev. Lett.* **120** (2018) 231801 [1804.02610].

[11] ATLAS collaboration, M. Aaboud et al., *Search for pair production of up-type vector-like quarks and for four-top-quark events in final states with multiple b-jets with the ATLAS detector*, *JHEP* **07** (2018) 089 [1803.09678].

[12] ATLAS collaboration, M. Aaboud et al., *Combination of the searches for pair-produced vector-like partners of the third-generation quarks at* $\sqrt{s} =$ *13 TeV with the ATLAS detector*, 1808.02343.

[13] CMS collaboration, A. M. Sirunyan et al., *Search for vector-like T and B quark pairs in final states with leptons at* $\sqrt{s} =$ *13 TeV*, 1805.04758.

[14] CMS Collaboration, *Search for* $t\bar{t}H$, $h \to b\bar{b}$ *production using the 2017 data sample*, CMS Analysis Note 2018/235, CERN, 2018. http://cms.cern.ch/iCMS/jsp/db_notes/noteInfo.jsp?cmsnoteid=CMS%20AN-2018/235.

[15] "Json file /afs/cern.ch/cms/CAF/CMSCOMM/COMM_DQM/certification/Collisions17/13TeV/ReReco/Cert_294927-306462_13TeV_EOY2017ReReco_Collisions17_JSON.txt."

[16] S. Alioli et al., *A general framework for implementing NLO calculations in shower Monte Carlo programs: the POWHEG BOX*, *JHEP* **06** (2010) 043 [1002.2581].

[17] J. Alwall, R. Frederix, S. Frixione, V. Hirschi, F. Maltoni, O. Mattelaer et al., *The automated computation of tree-level and next-to-leading order differential cross sections, and their matching to parton shower simulations*, *JHEP* **07** (2014) 079 [1405.0301].

[18] NNPDF collaboration, R. D. Ball et al., *Parton distributions from high-precision collider data*, *Eur. Phys. J. C* **77** (2017) 663 [1706.00428].

[19] T. Sjostrand, S. Ask, J. R. Christiansen, R. Corke, N. Desai, P. Ilten et al., *An Introduction to PYTHIA 8.2*, *Comput. Phys. Commun.* **191** (2015) 159 [1410.3012].

[20] CMS collaboration, V. Khachatryan et al., *Event generator tunes obtained from underlying event and multiparton scattering measurements*, *Eur. Phys. J. C* **76** (2016) 155 [1512.00815].

[21] P. Skands, S. Carrazza and J. Rojo, *Tuning PYTHIA 8.1: the Monash 2013 tune*, *Eur. Phys. J. C* **74** (2014) 3024 [1404.5630].

[22] "Instructions for applying electron and photon id." https://twiki.cern.ch/twiki/bin/view/CMS/EgammaIDRecipesRun2#Electron_efficiencies_and_scale.

[23] "Reference measurements and calibrations for run-ii." https://twiki.cern.ch/twiki/bin/view/CMS/MuonReferenceEffs2017.

[24] "Jet identification." https://twiki.cern.ch/twiki/bin/viewauth/CMS/JetID13TeVRun2017, r6.

[25] "Jet identification in high pile-up environment." https://twiki.cern.ch/twiki/bin/viewauth/CMS/PileupJetID#Information_for_13_TeV_data_anal.

[26] "Jet energy resolution." https://twiki.cern.ch/twiki/bin/view/CMS/JetResolution#JER_Scaling_factors_and_Uncertai, r54.

[27] CMS collaboration, A. M. Sirunyan et al., *Identification of heavy-flavour jets with the CMS detector in pp collisions at 13 TeV*, *JINST* **13** (2018) P05011 [1712.07158].

[28] CMS Collaboration, *Search for* $t\bar{t}H$, $h \to b\bar{b}$ *decays using the full 2016 data sample*, CMS Analysis Note 2017/063, CERN, 2017. http://cms.cern.ch/iCMS/jsp/db_notes/noteInfo.jsp?cmsnoteid=CMS%20AN-2017/063.

[29] G. Fox and S. Wolfram, *Event shapes in e+e- annihilation*, *Nuclear Physics B* **157** (1979) 543 .